
**Integral Data Evaluation
of Stainless Steel, ^{239}Pu , ^{240}Pu ,
and H_2O for Homogeneous
Plutonium Systems**

U. P. Jenquin
J. K. Thompson
T. J. Trapp
D. A. Kottwitz

August 1979

Prepared for
the U.S. Nuclear Regulatory Commission

Pacific Northwest Laboratory
Operated for the U.S. Department of Energy
by Battelle Memorial Institute



PNL-3071

POOR ORIGINAL

996 090

790926#226

NOTICE

This report was prepared as an account of work sponsored by an agency of the United States Government. Neither the United States Government nor any agency thereof, or any of their employees, makes any warranty, expressed or implied, or assumes any legal liability or responsibility for any third party's use, or the results of such use, of any information, apparatus product or process disclosed in this report, or represents that its use by such third party would not infringe privately owned rights.

POOR ORIGINAL

996 091

Available from
National Technical Information Service
Springfield, Virginia 22161

INTEGRAL DATA EVALUATION OF STAINLESS
STEEL, ^{239}Pu , ^{240}Pu , and H_2O FOR
HOMOGENEOUS PLUTONIUM SYSTEMS

U.P. Jenquin
J.K. Thompson
T.J. Trapp
D.A. Kottwitz

August 1979

Prepared for the Division of Safeguards,
Fuel Cycle and Environmental Research
Office of Nuclear Regulatory Research
U.S. Nuclear Regulatory Commission
Washington, D.C. 20555
Under Interagency Agreement DOE EY-76-C-06-1830
NRC FIN No. B2075

Pacific Northwest Laboratory
Richland, Washington 99352

996 092

EXECUTIVE SUMMARY

Theory-experiment correlations of plutonium-fueled systems using ENDF/B cross-section data have usually resulted in calculated neutron multiplication values which are several percent higher than measured values. The discrepancies could be due to cross-section data, theoretical methods, and/or interpretation of the experiment. We have performed neutronics analyses of homogeneous plutonium critical experiments to determine where some of the cross sections may be deficient. New thermal cross-section data (0-3 eV) were generated for ^{239}Pu and ^{240}Pu capture, fission, and neutrons per fission. Two scattering kernels for hydrogen bound in water were also generated. Calculated values of k_{eff} using this new data were compared with corresponding values using ENDF/B-IV data.

The results indicate that the ^{240}Pu resonance data is sufficiently well known for hydrogen-moderated plutonium systems. The data in the vicinity of the 0.3 eV ^{239}Pu resonance and the hydrogen-bound-in-water kernel were found to be very important in determining the multiplication of plutonium systems. As a result, it is recommended that additional cross-section measurements be made for ^{239}Pu to determine this data more accurately. Also, the two scattering kernels generated for this project should be refined and a more thorough evaluation of neutron scattering in water needs to be made utilizing experimental data and theoretical models currently available.

In systems using stainless steel as structural and/or neutron control, a large fraction of the neutron absorptions occur in the stainless steel. Therefore, the cross-section data for the components of stainless steel must be known quite accurately. Analyses of several systems containing stainless steel indicate that the uncertainty in calculated values of k_{eff} is small using current estimates of the uncertainties in the cross sections. Experiments more appropriate for the evaluation of stainless-steel data should be performed.

TABLE OF CONTENTS

EXECUTIVE SUMMARY	iii
INTRODUCTION	1
CALCULATIONAL MODEL	2
IMPROVED DATA	4
ALTERNATE NUCLEAR DATA FOR ^{239}Pu AND ^{240}Pu BELOW 3 eV	4
Theoretical Formalism	4
Neutron-Nucleus Interaction Theory	5
The Parameters of the Model	6
Summary of the Model	7
Fitting for ^{240}Pu	7
Fitting for ^{239}Pu	8
THE SCATTERING CROSS SECTION FOR HYDROGEN BOUND IN WATER	10
TISK Scattering Law	12
H ₂ O Scattering Law Based on Anisotropic Molecular Vibrations	14
Phonon Spectrum	20
ENDF Scattering Law	21
Comparison of Scattering Models	21
RESULTS	23
STAINLESS STEEL	23
REACTIVITY VALUES WITH ENDF/B-IV DATA	24
EFFECT OF CHANGING ^{239}Pu DATA	24
EFFECT OF CHANGING ^{240}Pu DATA	25
EFFECT OF CHANGING THE H ₂ O KERNEL	25
CONCLUSIONS AND RECOMMENDATIONS	28
REFERENCES	30

996 094

LIST OF FIGURES

1.	Ratio of New ^{240}Pu Data to ENDF/B-IV ^{240}Pu Data	51
2.	ENDF/B-IV Capture Data for ^{240}Pu	52
3.	ENDF/B-IV Absorption Cross Section for ^{239}Pu	53
4.	ENDF/B-IV Fission Cross Section for ^{239}Pu	54
5.	Ratio of New Data to ENDF/B-IV Data for ^{239}Pu Absorption	55
6.	Ratio of New Data to ENDF/B-IV Data for ^{239}Pu Fission	56
7.	ENDF/B-IV Production-to-Absorption Ratio for ^{239}Pu	57
8.	Ratio of Eta for New Data to Eta for ENDF/B-IV Data for ^{239}Pu	58
9.	Phonon Spectrum Used to Evaluate the Scattering Law for Hydrogen Bound in Water	59
10a.	Total Scattering Cross Section for Hydrogen Bound in Water	60
10b.	Total Scattering Cross Section for Hydrogen Bound in Water	61
11.	Transfer Cross Section from Group 173 for ENDF Hydrogen Bound in Water	62
12.	Transfer Cross Section from Group 173 for TISK Hydrogen Bound in Water	63
13.	Transfer Cross Section from Group 173 for TISK-Koppel Hydrogen Bound in Water	64
14.	Ratio of Transfer Cross Sections from Group 173 for Hydrogen Bound in Water	65
15.	Ratio of TISK-Koppel to TISK Transfer Cross Sections from Group 173	66
16.	Reactivity of Homogeneous Plutonium Systems Using ENDF/B-IV Data	67
17.	Reactivity Effect of New Data for ^{239}Pu	68
18.	Reactivity Effect of New Data for ^{240}Pu	68
19.	Reactivity Effect of Using TISK H_2O	69
20.	Comparison of TISK-Koppel to TISK	69

LIST OF TABLES

1.	25 Broad-Group Structure	32
2.	Homogeneous Plutonium Benchmarks	33
3.	Fundamental Theoretical Forms	34
4.	Combinations of Fundamental Theoretical Forms	35
5.	The Parameters of the Model	36
6.	Absolute Data for ^{240}Pu Used for Normalization	37
7.	Preliminary Results of ^{240}Pu Data Analysis	37
8.	Resonance Parameters from the Preliminary Fit of ^{239}Pu Data	38
9.	2200 m/s Parameters for ^{239}Pu	38
10.	Parameters for the Six Peaks of the Phonon Spectrum	39
11.	Comparison of H_2O Kernels for Broad Group 13	40
12.	Comparison of H_2O Kernels for Broad Group 14	40
13.	Comparison of H_2O Kernels for Broad Group 15	41
14.	Comparison of H_2O Kernels for Broad Group 16	41
15.	Comparison of H_2O Kernels for Broad Group 17	42
16.	Comparison of H_2O Kernels for Broad Group 18	42
17.	Comparison of H_2O Kernels for Broad Group 19	43
18.	Comparison of H_2O Kernels for Broad Group 20	43
19.	Comparison of H_2O Kernels for Broad Group 21	44
20.	Comparison of H_2O Kernels for Broad Group 22	44
21.	Comparison of H_2O Kernels for Broad Group 23	45
22.	Comparison of H_2O Kernels for Broad Group 24	45
23.	Comparison of H_2O Kernels for Broad Group 25	45

LIST OF TABLES (CONTINUED)

24.	Evaluation of Stainless Steel Using Homogeneous Plutonium Benchmarks	46
25.	Evaluation of Stainless Steel Using Enriched UO ₂ Lattice Benchmarks	46
26.	Description of Benchmarks Used to Evaluate Data Changes	47
27.	Group Fluxes for Benchmark 2 Using Various Water Kernels	47
28.	Group Fluxes for Benchmark 4 Using Various Water Kernels	48
29.	Group Fluxes for Benchmark 14 Using Various Water Kernels	49
30.	Reactivity Effect of Water Kernel on Leakage	50

996 097

ACKNOWLEDGEMENTS

Preliminary cross-section data for ^{239}Pu was least squares fitted on a project sponsored by the Electric Power Research Institute. Permission to use the data in this project prior to publication is greatly appreciated.

Appreciation is also expressed to M. A. Lewallen, R. T. Perry, and G. W. McNair for their technical contributions in the early stages of the project.

INTRODUCTION

Neutronics analyses of systems containing plutonium have demonstrated the need to improve the calculational methods and/or the cross-section data. For some plutonium systems the theory-experiment correlation has been very bad; outside of the range one would expect due to estimated uncertainties in methods and data. For other plutonium systems the theory-experiment correlation is much better than one would expect considering the uncertainties in methods and data.

In an attempt to improve the neutronics analysis of plutonium systems, the Nuclear Regulatory Commission (NRC) commissioned Battelle, Pacific Northwest Laboratory (PNL) to define where the neutron cross sections for the isotopes of plutonium on ENDF/B-IV can be improved. NRC's main interest was in application to criticality safety analysis of shipping spent light water reactor (LWR) fuels. Since stainless steel is used structurally in shipping casks and is a good neutron poison, NRC also requested an assessment of the adequacy of ENDF/B-IV data for the constituents of stainless steel.

The first task of the project was to define a set of integral benchmark experiments.⁽¹⁾ These have been documented in NUREG/CR-210 (Benchmark Experiments to Test Plutonium and Stainless Steel Cross Sections). In this report we assess the accuracy of ENDF/B-IV plutonium and stainless steel cross sections. A selected portion of the benchmarks in NUREG/CR-210 were used in the analyses.

CALCULATIONAL MODEL

The principal calculational tools consist of the NITAWL, XSDRNPM, and KENO-IV codes⁽²⁾ and a 25-group cross section set which was collapsed from a 218-group ENDF/B-IV set⁽³⁾ generated by Oak Ridge National Laboratory (ORNL). The 25-group structure is given in Table 1. This calculational model is what ORNL had been using for criticality safety analyses at the time we initiated our calculations. Our version of NITAWL performs a NIT⁽⁴⁾ calculation down to 3.05 eV. Recently ORNL has gone to a NIT calculation down to 0.5 eV. They have also added 2 groups at high energies and reprocessed some of the cross sections. These differences lead to minor changes in calculated reactivity value but have a negligible impact on relative differences. Hence, small changes in the methods do not affect our conclusions.

XSDRNPM was used to calculate the systems amenable to one-dimensional analysis. For the remaining systems KENO-IV was used. Comparisons between ENDF/B-IV cross sections and alternate data sets were done only for the systems calculated with XSDRNPM. The differences are of the order (or smaller) of the uncertainty in the KENO-IV results, hence it is not possible to draw conclusions for the more complicated systems.

The plutonium benchmarks used in the correlations are summarized in Table 2. A wide range of H/Pu atom ratios is covered. The ²⁴⁰Pu content also covers a wide range; however, it would have been desirable to have more systems with a high ²⁴⁰Pu content (>20%). A more detailed description of the benchmarks is given in Reference 1.

Two pair of benchmarks were used to test stainless steel cross sections. A comparison between the two systems gives information on the stainless steel cross sections. Benchmarks 15a and 15b (see Table 2) are homogeneous reflected plutonium systems. The stainless steel wall is thicker in Benchmark 15b. The reactivity effect due to the extra stainless steel is compensated by a slight change in the solution composition. The other pair of benchmarks used for stainless steel evaluation consist of lattices fueled with UO₂. The same fuel is used in each benchmark. Benchmark 42b has aluminum clad while 42a has stainless steel clad. The difference in reactivity is compensated by a change in the number of fuel rods required for criticality.

Six of the homogeneous plutonium benchmarks (those with an asterisk in Table 2) were selected to be reanalyzed with alternate data in an attempt to determine the sensitivity of the results to different evaluations of the data. The reanalysis was accomplished by substituting each set of alternate data for the ENDF/B-IV data, one set at a time.

996 101

IMPROVED DATA

The data identified to have the greatest effect in calculating plutonium-fueled thermal systems consists of: ^{239}Pu capture, fission, and neutron production; ^{240}Pu capture due to the 1 eV resonance; and the thermal scattering cross section for water. The source of the alternate data sets is described below.

ALTERNATE NUCLEAR DATA FOR ^{239}Pu AND ^{240}Pu BELOW 3 eV

Alternate evaluations for ^{239}Pu and ^{240}Pu below 3 eV were taken from preliminary studies in which selected differential experimental nuclear data for these isotopes were fitted with a non-linear parameter estimation technique.⁽⁵⁾ After briefly reviewing the formalism, the results of the investigations for each isotope will be discussed.

Theoretical Formalism

The evaluation technique is essentially nonlinear-weighted least-squares fitting. As such its range of validity is restricted by the two implicit assumptions on the statistical nature of the data inherent to all least-squares analysis, viz:

- . The data are not subject to significant systematic bias ($\hat{\mu} = \mu$)
- . All data are samples from a common population (σ^2 is a constant)

One further caveat concerning least-squares analysis is that a single flyer (datum "distant" from theory) can induce non-trivial local perturbations of the theory. If the data to be fitted do not meet the assumptions or exhibit flyers, the model used to describe the data must be formulated in such a way as to compensate for these deficiencies.

Unfortunately, experimental nuclear data may fail on all counts. Systematic bias may be induced by normalization errors or energy-scale errors. It is not uncommon for flyers to be present. Finally, due to differences in reporting by different experimenters, uncertainty measures, if they are reported at all, may reflect total uncertainties or only certain components of

the total uncertainty. Hence, data from different experiments may exhibit widely disparate variances.

To minimize the effects of systematic bias, each data set is allowed three experimental parameters to adjust the normalization and energy-scale for those data within that data set. These parameters are not required, but if they are present, they are treated on a par with the theory parameters. An internal weight-adjustment scheme may be used to down-weight flyers and to balance the variances between data sets to satisfy the common population assumption. However, taking such liberties with reported data is not to be taken lightly, for it introduces a new set of complications. First, it forces one to work with an implicit relation between measurement and theory rather than the more common case of an explicit theory. Second, data which were in principle originally statistically independent are now correlated, and correlation introduces complexity in any statistical analysis. The first complication is one of mechanical detail. The second complication is actually an illusion. If the experimental parameters are statistically significant, the original data in fact were not statistically independent for they exhibit a common systematic bias. Indeed, the correlation is shifted from the measurement-space to the parameter-space, leaving the data essentially statistically independent. Furthermore, since the correlation effects are now contained in the parameter-space, a modest sophistication of the residuals analysis yields more rigorous results than could be obtained in the absence of experimental parameters.

Neutron-Nucleus Interaction Theory

The ultimate goal is to describe the thermal energy region nuclear interactions by fitting experimental data as just described to analytic theoretical forms derived from neutron-nucleus interaction theory. There are a limited number of nuclear interactions of interest in the thermal range, all of which may be constructed from three fundamental theoretical forms (Table 3). A modified Adler-Adler formalism is used to describe fission and capture cross sections; while coherent, incoherent, and total scattering are described by the multi-level Breit-Wigner formalism. Finally, an unnamed spin-dependent resonance formalism had to be invented to model data forms

involving ν because of the energy-dependence of ν in the thermal energy range. Absorption and total cross sections and the ratios of interest may be constructed from these fundamental theoretical forms as shown in Table 4. Using the same construction logic, any theoretical form may be combined with any second theoretical form that does not involve ν in two-component sums and ratios. This feature allows simultaneous multi-isotope fitting when there exist data dependent upon two isotopes such as a limited purity sample with a single contaminant (e.g., ^{239}Pu with ^{240}Pu contaminant) of data measured relative to a standard with non-trivial shape uncertainty (e.g., $\sigma_f^{49}/\sigma_f^{25}$).

One of the primary reasons for choosing these theoretical forms is the commonality of physical theory parameters between forms. The whole purpose of performing simultaneous fitting would be lost were this commonality absent, for there would then be no competing constraints to compromise. Indeed, in some cases it is only through these competing constraints that some parameters are even marginally determinable. Furthermore, one can obtain indirect evidence of conflicting data when parameters become unphysical or exhibit large uncertainties due to these competing constraints.

The Parameters of the Model

Now that both the theory forms have been described, a complete list of the parameters can be tabulated (see Table 5). Obviously, in any real problem, the number of parameters could be fairly large. In general, the quality and quantity of data are inadequate to determine all of these parameters, especially when there is a high degree of correlation between some of them. Furthermore, some of the parameters are generally known with fair accuracy from prior evaluations, and expediency demands that some use be made of this *a priori* knowledge. In our model there are two methods available by which this information can be used to limit the region of parameter-space to be searched. The first method is the case of setting a parameter to a fixed constant. In preliminary fitting in particular, where one may be interested in examining data for systematic bias, this option is very useful. Conversely, in the final stages of fitting, one would like to determine as many parameters as possible from the data alone, but subject to restricting the range of certain of the parameters to values which are physically

plausible or which are demonstrably optimal from evidence of prior fitting. The second method allows one to do just that by treating a parameter estimate which has an associated uncertainty as a datum. Consequently, although the full dimensionality of the parameter-space is used, there are constraints which limit the freedom of parameter variation in some dimensions.

Summary of the Model

In the non-linear parameter estimation technique we used, the data are transformed via theory to remove systematic bias attributable to normalization or energy-scale errors. Weight-adjustment may be used if necessary to satisfy the common variance assumption. A collection of theoretical forms derived from neutron-nucleus interaction theory based on a common set of physical parameters has been chosen to provide competing constraints in fitting the various data forms. There is arbitrary freedom in choosing which parameters are to be varied and which are to remain fixed in the fitting algorithm. Furthermore, any subset of the variable parameters may be constrained, forcing each parameter of the subset to lie in the neighborhood of its *a priori* estimate.

Fitting for ^{240}Pu

The low-energy region in ^{240}Pu is dominated by the 1 eV resonance, but to accurately model the region a bound level and the 20 eV resonance were included in the fit with all parameters fixed, the bound level as a mirror image of the 20 eV resonance. The data base used in the studies include the capture data of Weston and Todd,⁽⁶⁾ the total data of Leonard, et. al.,⁽⁷⁾ and Block,⁽⁸⁾ and normalization points (see Table 6) for capture,⁽⁹⁾ scattering⁽¹⁰⁾ and fission.⁽¹¹⁾ The total data of Leonard through the resonance were corrected for Doppler broadening, and on advice from Leonard the energy scale was allowed to adjust. The capture data of Weston and Todd show evidence of ^{239}Pu contaminant and were fit as the sum of ^{240}Pu capture and ^{239}Pu capture with the impurity concentration of ^{239}Pu being an adjustable parameter. Both of these data sets, along with Block's total data, were allowed to renormalize. Furthermore, the data set weights of these three data sets were internally adjustable. This was especially important for the Weston and Todd capture data, since in the absence of measurement uncertainties, the data weights were ar-

bitrarily set to correspond to a 5% data uncertainty with internal adjustment of the data weights allowed. The preliminary results for the 2200 m/s zero-kelvin cross sections and the parameters of the 1 eV resonance are shown in Table 7. The cross sections generated using these parameters were Doppler-broadened to 293.6K, weighted with a 293.6K Maxwellian spectrum to 5 kT (~ 1.275 eV) and a 1/E spectrum above 5 kT, and integrated to obtain group-averaged cross sections in the 78 thermal fine groups (10^{-5} to 3.05 eV). The resonance integral (from 0.8 to 1.3 eV) is 1.9% larger than the ENDF/B-IV value.

The ratio of this data to ENDF/B-IV data is shown in Figure 1. The large spike at 0.5 eV is probably due to an error in processing the ENDF/B-IV data. This error is not significant in reactivity calculations, because the cross section is small at this energy (Figure 2). The unusual shape at 1 eV is due to a small shift in the location of the resonance.

Fitting for ^{239}Pu

Fitting the low-energy nuclear data for ^{239}Pu is complicated by the importance of a strong bound level just below zero neutron energy, the evidence of energy-dependence for ν and non-negligible Doppler-broadening effects in the visible level at ~ 0.3 eV. Furthermore, the experimental differential data sets anticipated to be the most significant do not seem to be in agreement, which leads to biased fits compromising the integrity of least-squares analysis. This apparent disagreement may be the result of several inter-related factors, such as

- Sample contamination by higher Pu isotopes, especially ^{240}Pu and ^{241}Pu (along with ^{241}Am daughter)
- Misinterpretation of reported uncertainty measures
- Unaccounted for resolution effects
- Slight differences in the reported energy-scale
- Inadequacy of the theoretical model.

Care has been taken to minimize the effects of each of these by using the very general theoretical model described above (which includes a theoretical method for data adjustment).

The alternate ^{239}Pu nuclear data used in this study were taken from preliminary fitting results whose range did not extend to 3 eV. However, the extrapolation of the fit is acceptable for reactor calculations, for the only cross section poorly represented (radiative capture >1.5 eV) is of little consequence over the range of its extrapolation. Table 8 shows the parameters of the preliminary data analysis, while Figures 3-7 exhibit group-averaged values. The discontinuities just below 1 eV appear to be due to a processing error in the ENDF/B-IV data, but are inconsequential for the reactor calculations presented in this report.

Figures 3 and 4 show 78-group values of the ENDF/B-IV absorption and fission cross section taken from the ORNL processed library. The ratio of the new data relative to ENDF/B-IV data is shown in Figures 5 and 6 for absorption and fission, respectively. Figure 7 shows the production-to-absorption ratio (η) derived from the ENDF/B-IV data. Shown in Figure 8 is the ratio of η for the preliminary fit to η for ENDF/B-IV data. Note the increase in the vicinity of 0.3 eV and the increase above 0.8 eV. The latter increase reflects a significantly different interpretation of the ^{239}Pu capture cross section in the region subject to large uncertainties due to ^{240}Pu contamination and is not inconsistent with the measured η data on the falling side of the resonance. No attempt is made here to assign uncertainties to the alternate data, since they result from a biased fit and have been forced to produce the best estimate thermal zero-kelvin cross sections indicated in Table 8.

Two notable features of these results are the upward revision of the thermal fission cross section and the variation of ν with energy in the thermal range. The change in the fission cross section is due almost entirely to recent measurements of the ^{239}Pu half-life⁽¹²⁾ (generally used for sample assay of Pu foils) leading to an estimate of $T_{1/2} = 24134 \pm 8$ yr in contrast to the commonly used value of $T_{1/2} = 24395 \pm 10$ yr. This revision of $T_{1/2}$ corresponds to $\sim 1.1\%$ increase in the normalization of fission data where the sample assay was determined by α -counting. The variation of ν with energy, fitted to recent measurements,^(13, 14, 15) indicates a drop of $\sim 1\%$ from the lowest energy measurements (a few meV) to the peak at 0.3 eV with recovery to the first value at higher energies. Introduction of energy variation in ν

helps to explain the differences between monoenergetic neutron η measurements and the ratio of cross sections, σ_f/σ_a .

The 2200 m/s parameters resulting from the new fit are compared with ENDF/B-IV data in Table 9. The ratio of neutrons produced per neutron absorbed (η) is a good indicator of the reactivity effect. It has increased only 0.23%.

THE SCATTERING CROSS SECTION FOR HYDROGEN BOUND IN WATER

The scattering of low-energy neutrons involves not only the nuclear properties of the scattering nucleus, but also the dynamics of the molecule. The hindered rotations, translations, and vibrations of the molecule in a bound system are important contributors to the scattering process. An analysis of the scattering cross section must include these effects.

The scattering cross section is composed of both a coherent and an incoherent component. The incoherent component of the scattering cross section describes the dynamics of a single molecule in the bound system. The coherent component of the scattering cross section describes the correlated dynamics of the system of molecules. For water, the coherent component composes approximately 2% of the total scattering.

Models which treat scattering as completely incoherent will provide a reasonable representation of the behavior of scattering in water, and permit calculational simplifications. The scattering cross section per hydrogen atom in water using the incoherent scattering approximation can be written as

$$\sigma_s(E \rightarrow E', \mu) = \frac{\sigma_b}{4\pi kT} \left(\frac{E'}{E} \right)^{1/2} e^{-B/2} S(\alpha, \beta) \quad (1)$$

where

$\sigma_s(E \rightarrow E', \mu)$ = the differential scattering cross section (barns/ev-steradian)

σ_b = the bound atom scattering cross section

k = the Boltzmann constant

T = the temperature of the scattering system

E	=	initial energy
E'	=	final energy
μ	=	cosine of the scattering angle
$S(\alpha, \beta)$	=	the scattering law

In this expression α and β are the square of the momentum transfer and energy transfer in dimensionless units. They are related to the initial and final neutron energies and the systems temperature by

$$\alpha = \frac{E + E' - 2\mu\sqrt{EE'}}{AKT} \quad (2)$$

$$\beta = \frac{E' - E}{kT}$$

where

A = the mass of the scattering atoms divided by the neutron mass.

The expression for the scattering cross section depends only on the scattering law and known numerical factors. Given a form for the scattering law, the cross sections which are needed in reactor analysis can be determined. The entire problem of evaluating thermal neutron scattering becomes a matter of evaluating the scattering law.

Many different techniques have been used to evaluate the scattering law. Each technique differs in basic data, theoretical assumptions, and numerical methodology. The differences in any of these areas can produce a different evaluation.

In this study three different evaluations of the scattering law were used. They are for convenience denoted as TISK, TISK-Koppel, and GASKET. All of the evaluations use the same basic assumption. This assumption is that the dynamics of a molecule in a bound system can be expressed in terms of a phonon spectrum. The TISK and TISK-Koppel evaluations are both new. The GASKET evaluation is the evaluation provided in the ENDF/B-IV data file.

Since the purpose of this work was to investigate the sensitivity of integral experiments to the scattering cross section, an effort was made to eliminate the sensitivity of the scattering cross section to the details of the processing and handling routines. The evaluated scattering laws were calculated on the same numerical grid as the present ENDF/B-IV values.

Both new evaluations were processed into a 78-group set of cross sections using the FLANGE-II⁽¹⁶⁾ computer code. Each of the three scattering laws and the phonon spectrum are described separately.

TISK Scattering Law

The scattering law in the TISK⁽¹⁷⁾ formulation is written as

$$S(\alpha, \beta) = \frac{1}{\pi} \int_0^{\infty} e^{-\alpha W(t)} \cos(\beta t) dt \quad (3)$$

where $W(t)$ is a width function related to the mean squared displacement of an atom from its initial position.

The width function can be expressed in terms of the fundamental parameter of a bound system, the phonon spectrum, as

$$W(t) = \int_0^{\infty} \rho(\beta) \left[\frac{\cosh(\beta/2) - \cos(\beta t)}{\beta \sinh(\beta/2)} \right] d\beta \quad (4)$$

where

$$\rho(\beta) = \text{the phonon spectrum.}$$

No restriction has been placed on the form of the phonon spectrum in (4). In general, it can be any representation which describes the dynamics of the molecular system. Most functional representations require a numerical evaluation of the integral in (4).

In the TISK method, the Lindermeier-Gibbs form of the phonon spectrum is used. This form is a series of modulated Gaussian peaks. The representation allows flexibility in modeling the peaks and valleys of the phonon

spectrum, which correspond to the hindered rotations, vibrations, and translations of the molecule, while allowing an analytic integration of (4).

The phonon spectrum in the Lindenmeier-Gibbs formulation can be written as

$$\rho(\beta) = \rho_0(\beta) + \sum_{i=1}^N \frac{F_i \beta \sinh(\beta/2)}{2\sqrt{\pi\delta_i}} e^{-\delta_i/4} \left[\frac{e^{-(\beta-\gamma_i)^2/4\delta_i} + e^{-(\beta+\gamma_i)^2/4\delta_i}}{\gamma_i \sinh(\gamma_i/2) + \delta_i \cosh(\gamma_i/2)} \right] \quad (5)$$

where γ_i and δ_i are parameters which describe the resonance-like peaks of the spectrum, and F_i is a weighting factor which represents the fractional contribution of a particular peak to the spectrum.

The term $\rho_0(\beta)$ accounts for the diffusive motion of the system. For a solid this form is zero. For a gas it is a delta function. For a liquid the exact form is not known, but Egelstaff and Schofield⁽¹⁸⁾ have recommended the form

$$\rho_0(\beta) = \frac{0.16}{\pi} \frac{\sinh(\beta/2)}{\beta} (\beta\sqrt{10^4 + 0.25}) K_1(\beta\sqrt{10^4 + 0.25}) \quad (6)$$

where K_1 is a Bessel function.

Equation (4) can be integrated to give

$$W(t) = W_0(t) + \sum_{i=1}^N F_i [A_i - B_i e^{-\delta_i t^2} \cos(\gamma_i t)] \quad (7)$$

where

$$A_i = \frac{\cosh(\gamma_i/2)}{\gamma_i \sinh(\gamma_i/2) + \delta_i \cosh(\gamma_i/2)}$$

$$B_i = \frac{e^{-\delta_i/4}}{\gamma_i \sinh(\gamma_i/2) + \delta_i \cosh(\gamma_i/2)}$$

996 111

and

$$W_0(\epsilon) = 0.08 [(c^2 + 10^4 + 0.25)^{1/2} - 100]$$

This eliminates the necessity of performing two numerical integrations. The integral in (3) must still be performed numerically to determine the scattering law from the displacement function. This integral is ideally suited for evaluation using extremely fast and accurate fast-Fourier transform techniques.⁽¹⁹⁾

These techniques were incorporated in the TISK computer code. For large values of the energy and momentum transfer an asymptotic expansion was used to evaluate the scattering law.

H₂O Scattering Law Based on Anisotropic Molecular Vibrations

In order to provide an additional H₂O scattering kernel for sensitivity calculations, the Lindenmeier-Gibbs (L-G) formalism employed in program TISK⁽¹⁷⁾ was modified to take into account the anisotropy of the molecular vibrations. For this purpose Koppel's simplified dynamical model of H₂O vibrations⁽²⁰⁾ was adapted to the L-G formalism by assuming that each of the L-G modulated Gaussian peaks in the phonon spectrum can be associated uniquely with one of Koppel's modes (stretching, bending, hindered rotation or hindered translation). In principle the combined TISK-Koppel formalism should be a refinement of the standard TISK formalism,⁽¹⁷⁾ which is based on the assumption of isotropic vibrations, and Koppel's original work,⁽²⁰⁾ which employed Nelkin's delta-function phonon spectrum and an axially symmetric distribution of polarization vectors.

The scattering law averaged over all orientations of the water molecule is

$$\langle\langle S(\alpha, B) \rangle\rangle = \frac{1}{\pi} \int_0^\infty dt \langle\langle \exp[-\alpha W(t)] \rangle\rangle \cos(Bt) \quad (8)$$

where S is the scattering law for an arbitrary molecular orientation

$W(t)$ is the corresponding width function (dependent on orientation)

α and β have been defined previously

and $\langle\langle Z \rangle\rangle$ = average of Z over all orientations.

Instead of working directly with equation (8), we adopt the method used in Reference 17 to improve the accuracy of integration at large values of t . The averaged scattering law is rewritten as

$$\langle\langle S(\alpha, \beta) \rangle\rangle = \langle\langle S(\alpha, \beta) \rangle\rangle_1 + \langle\langle S(\alpha, \beta) \rangle\rangle_2 \quad (9)$$

where

$$\langle\langle S(\alpha, \beta) \rangle\rangle_1 = \frac{1}{\pi} \int_0^\infty dt \langle\langle \exp[-\alpha W_\infty(t)] \rangle\rangle \cos(\beta t) \quad (10)$$

$$\langle\langle S(\alpha, \beta) \rangle\rangle_2 = \frac{1}{\pi} \int_0^\infty dt \langle\langle \exp[-\alpha W(t)] - \exp[-\alpha W_\infty(t)] \rangle\rangle \cos(\beta t) \quad (11)$$

$W_\infty(t)$ = asymptotic (large t) form of $W(t)$.

There are now two Fourier transforms, but the one in equation (10) can be done analytically due to the simple form of $W_\infty(t)$. Indicating the orientation dependence of $W(t)$ explicitly, we have

$$W(t, \phi, \theta) = W_d(t) + W_c(\phi, \theta) + W_T(t, \phi, \theta) \quad (12)$$

where $W_d(t)$ is the isotropic diffusion component, $W_c(\phi, \theta)$ is the time-independent component due to vibratory modes, and $W_T(t, \phi, \theta)$ is the time decaying component due to vibratory modes.

Thus we have

$$W_\infty(t) = W_d(t) + W_c(\phi, \theta) \quad (13)$$

Suppressing the independent variables, we have

$$\langle\langle S \rangle\rangle_1 = \langle\langle \exp[-\alpha W_c] \rangle\rangle \frac{1}{\pi} \int_0^\infty dt \exp[-\alpha W_d] \cos(\beta t) \quad (14)$$

$$\langle\langle S \rangle\rangle_2 = \frac{1}{\pi} \int_0^\infty dt \exp[-\alpha W_d] \left\{ \langle\langle \exp[-\alpha(W_c + W_T)] \rangle\rangle - \langle\langle \exp[-\alpha W_c] \rangle\rangle \right\} \cos(\beta t) \quad (15)$$

The explicit formulas for the components of $W(t)$ are

$$W_d(t) = 2d [(t^2 + c_0^2 + 0.25)^{1/2} - c_0] \quad (16)$$

where d and c_0 are known constants related to diffusion,

$$W_c(\phi, \theta) = e' + a \sin^2\theta \cos^2\phi + b \sin^2\theta \sin^2\phi + c \cos^2\theta \quad (17)$$

where θ and ϕ are suitable spherical polar coordinates

c = largest of quantities a' , b' and c'

b = intermediate of quantities a' , b' and c'

a = smallest of quantities a' , b' and c'

$$a' = 3A_s F_s$$

$$b' = A_r F_r + 3 \sum_{b=1}^2 A_b F_b$$

$$c' = 2A_r F_r$$

$$e' = \sum_{t=1}^2 A_t F_t$$

$$W_c(\phi, \theta) + W_T(t, \phi, \theta) = e'' + \underline{a} \sin^2\theta \cos^2\phi + \underline{b} \sin^2\theta \sin^2\phi + \underline{c} \cos^2\theta \quad (18)$$

where

\underline{c} = largest of quantities a'' , b'' and c''

\underline{b} = intermediate of quantities a'' , b'' and c''

\underline{a} = smallest of quantities a'' , b'' and c''

$$\begin{aligned}
a'' &= a' - 3B_s f_s(t) F_s \\
b'' &= b' - B_r f_r(t) F_r - 3 \sum_{b=1}^2 B_b f_b(t) F_b \\
c'' &= c' - 2B_r f_r(t) F_r \\
e'' &= e' - \sum_{t=1}^2 B_t f_t(t) F_t \\
f_i(t) &= \exp(-\delta_i t) \cos(\gamma_i t) \quad i = s, b, r, t
\end{aligned}$$

Subscripts s, b, r, t indicate stretching, bending, rotational, translational mode peaks.

A_i , B_i , γ_i , and δ_i are L-G parameters for the i-th mode peak.

F_i = weight of the i-th mode peak.

It is explicitly assumed here that there are 2 low energy translational peaks, 1 medium energy rotational peak, 2 medium energy bending peaks, and 1 (consolidated) high-energy stretching peak for H_2O .

Using the explicit formulas for the width components in equations (16), (17) and (18) we can exhibit final formulas for $\langle\langle S \rangle\rangle_1$. Let

$$\langle\langle S \rangle\rangle_1 \equiv QS_d \quad (19)$$

where

$$\begin{aligned}
Q &\equiv \langle\langle \exp[-\alpha W_c] \rangle\rangle \\
S_d &\equiv \frac{1}{\pi} \int_0^\infty dt \exp(-\alpha W_d) \cos(\beta t)
\end{aligned}$$

The formula for S_d can be integrated analytically to give

$$S_d = \frac{T \exp(Tc_0) x K_1(x)}{\pi(T^2 + \beta^2)} \quad (20)$$

where

$$T = 2d \alpha$$

$$x = \sqrt{(c_0^2 + 0.25)(T^2 + \beta^2)}$$

K_1 is a Bessel function

The orientation-averaged quantity Q can be written as a double integral

$$Q = \frac{1}{4\pi} \int_0^{2\pi} d\phi \int_{-1}^1 d(\cos\theta) \exp[-\alpha W_c(\phi, \theta)]$$

where $W_c(\phi, \theta)$ is defined in equation (17). The integral over θ can be done analytically to yield

$$Q = \frac{\exp[-\alpha(e' + c)]}{4\sqrt{\pi}} \int_0^{2\pi} d\phi \frac{\exp(\alpha q) \operatorname{erf}\sqrt{\alpha q}}{\sqrt{\alpha q}} \quad (21)$$

where

$$q \equiv c - b + (b - a)\cos^2\phi$$

The remaining integral over ϕ is done numerically by trapezoidal integration.

The integrand for $\langle\langle S \rangle\rangle_2$ in equation (15) includes Q and another orientation-averaged quantity $P(t)$ defined by

$$P(t) \equiv \langle\langle \exp[-\alpha(W_c + W_T)] \rangle\rangle \quad (22)$$

Again, the integration over θ can be performed analytically to yield

$$P(t) = \frac{\exp(-\alpha[e'' + \underline{c}])}{4\sqrt{\pi}} \int_0^{2\pi} d\phi \frac{\exp(\alpha p) \operatorname{erf}\sqrt{\alpha p}}{\sqrt{\alpha p}} \quad (23)$$

where

$$p(t) \equiv \underline{c} - \underline{b} + (\underline{b} - \underline{a})\cos^2\phi$$

The integral in equation (23) is done numerically by trapezoidal integration, and the cosine transform in equation (15) is done by a Fast Fourier Transform subroutine.

The numerical cosine transform method just described gives inaccurate results for large values of β . Thus it is necessary to supplement it with an alternative formulation. Although the saddle point method used in Reference 18 would probably be more accurate for this purpose, it was thought to be easier and quicker to formulate a generalization of the short collision time method used in program FLANGE-II.⁽¹⁶⁾ The method uses the scattering law for a free gas at an effective temperature related directly to the phonon spectrum of the scattering material. The formula for a material having isotropic vibrations is

$$S_{\text{sct}}(\alpha, \beta, R) = \frac{\exp\left[\frac{\beta}{2} - \frac{(\alpha - \beta)^2}{4\alpha R}\right]}{\sqrt{4\pi\alpha R}}, \quad \beta > 0 \quad (24)$$

where

$$R = T_{\text{eff}}/T$$

In the L-G formalism the temperature ratio is

$$R = \sum_i \frac{F_i}{2} \int_0^\infty d\beta \beta \coth(\beta/2) \rho_i(\beta) \quad (25)$$

where $\rho_i(\beta)$ are the normalized L-G peak functions.

For an anisotropic oscillator the ratio R is orientation dependent since the factor F_i is replaced by $F_i \Gamma_i(\phi, \psi, \theta)$. For the simplified Koppel dynamical model for H_2O the formulas for Γ_i for the various modes of vibration are

$$\Gamma_s = 3 \cos^2 \theta \quad (26)$$

$$\Gamma_b = 3 \cos^2 \phi$$

996 117

$$\Gamma_r = \cos^2\phi + 2 \cos^2\psi$$

$$\Gamma_t = \Gamma_d = 1,$$

where the subscripts s, b, r, t, d indicate stretching, bending, rotational, translational, and diffusive modes, and ϕ , ψ , θ are angles relative to x, y, z axes.

Since we could not perform the orientational integrations analytically, we approximated the double integral by a weighted sum of integrand values calculated for a preselected set of directions (or points on a unit sphere).⁽²¹⁾ Actually 2 different schemes were tested and found to give equivalent results. They are the 72-point 14th-degree formula of McLaren and the 128-point 15th-degree spherical product Gauss formula (FORTRAN functions S3S14 and S3S15 of Reference 21). Thus the final formula for the averaged short collision time scattering law is

$$\langle\langle S_{\text{sct}}(\alpha, \beta) \rangle\rangle = \sum_j w_j S_{\text{sct}}(\alpha, \beta, R_j) \quad (27)$$

where j is the index of directions specified by angles θ_j and ψ_j , and w_j is the corresponding weight.

Phonon Spectrum

In order to evaluate the scattering law for water in both the TISK and TISK-Koppel models, a phonon spectrum must be available. The experimental data of both Harling⁽²²⁾ and Haywood⁽²³⁾ for the phonon spectrum of hydrogen bound in water were combined. The Harling data was used for beta greater than 2.5 and the Haywood data for small beta. The experimental phonon spectrum was fitted using the nonlinear least squares techniques of the LEARN⁽²⁴⁾ computer code. Table 10 displays the values of the parameters for a 5-peak representation. An additional high-energy peak is included for the unresolved vibrational modes at a beta of 18. Figure 9 shows both the experimental and the functional evaluation of the phonon spectrum.

996 118

ENDF Scattering Law⁽²⁵⁾

The scattering law for H₂O was calculated for ENDF with the GASKET⁽²⁶⁾ computer code based on a model which retained the essential features of the Nelkin model. Between 0.04 and 0.165 eV the single delta function oscillator of the Nelkin model was replaced with a broad band of distributed modes for the hindered rotations. The data for the band of hindered rotations was taken from the work of Haywood.⁽²³⁾ Below 0.04 eV it was smoothly joined to a parabola. The original spectrum given by Haywood showed several peaks in this low-frequency range, corresponding to translational vibrations of the H₂O molecule as a whole. These modes were replaced by free translations of weight 1/18 in order to avoid numerical difficulties. The discrete internal modes of vibration of the H₂O molecule were taken from the Nelkin model with weights of 1/6 for the 0.205 eV mode and 1/3 for the 0.48 eV oscillator. The torsional band was then normalized to 4/9 in order to give the proper overall normalization.

Comparison of Scattering Models

The three different evaluations of the scattering cross section for a single hydrogen atom bound in a water molecule are displayed in Figures 10a and 10b. Both the TISK and TIKS-Koppel evaluations appear to be approximately 10% low in reproducing the cross section in the 1 to 3 eV range. At the other end of the spectrum (low energy) both the TISK and TISK-Koppel models are high in reproducing the scattering cross section. From 0.1 to 1.0 eV the three evaluations all reproduce the scattering cross section reasonably well.

Figures 11, 12, and 13 display the differential scattering cross section for fine group 173 (1.09-1.10 eV) from ENDF, TISK, and TISK-Koppel. Only the down scattering portion of the cross section is shown since the upscattering is related to the downscattering by detailed balance. The in-scattering contribution is much larger in both the TISK and TISK-Koppel models than the ENDF model.

Figure 14 shows the ratio of the TISK and TISK-Koppel scattering models to the ENDF model. The differences in the structure of the differential scattering from both TISK and TISK-Koppel can be seen in the ratio graphs.

The ratio of TISK-Koppel to TISK scattering is shown in Figure 15. The deviation from 1.0 is a representation of the anisotropy effect. The broad-group transfer cross sections (barns/atom) for the three water kernels for the 25-group structure are displayed in Tables 11 to 23. From these tables it is apparent that the phenomenon seen in fine-group 173 does not hold for all other groups.

RESULTS

STAINLESS STEEL

Reactivity values for Benchmarks 15a and 15b (homogeneous plutonium spheres) were determined with XSDRNPM. A summary of the results and a brief description of each system are given in Table 24. Each system is reflected with water, thus a portion of the neutrons thermalized in the reflector are absorbed in the stainless steel shell. As the shell thickness is increased the fraction of neutrons absorbed in the shell is increased as shown on line 5. The k_{eff} values given in Table 24 indicate that the absorption rate in the shell is too high because k_{eff} decreases as the shell thickness increases. Assuming other parameters are calculated accurately, the stainless steel absorption rate would have to decrease 8% to obtain identical k_{eff} values.

Reactivity values for Benchmarks 42a and 42b lead to an opposite conclusion as to the stainless steel cross sections. These benchmarks are enriched UO_2 lattices using the same fuel at the same lattice pitch. One has stainless steel clad while the other has aluminum clad. The results are summarized in Table 25. The reactivity effect of changing the clad is compensated by changing the core size; and hence, the neutron leakage from the system. The k_{eff} values given in Table 25 indicate that the absorption rate in the stainless steel is too low because k_{eff} increases as aluminum is replaced by stainless steel. If other parameters are calculated accurately or have cancelling effects, the absorption rate in stainless steel would have to increase by 9% to obtain identical k_{eff} values. Since the leakage fraction is quite different for the two systems, an error in the leakage calculation would lead to an erroneous conclusion.

Based on the results for the two pairs of benchmarks, no conclusion can be drawn as to the adequacy of stainless steel cross sections. Reported cross-section uncertainties for the constituents result in an uncertainty of less than 2% for the 2200 m/s cross section of stainless steel and an uncertainty of 10% for the resonance integral of stainless steel. For the lattices, 85% of the stainless steel absorptions are in the thermal energy range while for the solutions 98% of the absorptions are in the thermal energy range. The spread in range of composition of stainless steel leads to a larger spread

in the 2200 m/s cross section than the uncertainty due to cross-section measurements.

REACTIVITY VALUES WITH ENDF/B-IV DATA

Reactivity values for all of the homogeneous plutonium benchmarks given in Reference 1 were obtained with NITAWL and either XSDRNPM or KENO-IV using 25-group ENDF/B-IV cross sections. The results are shown in Figure 16 as a function of H/Pu ratio. Values of k_{eff} are $\sim 2\%$ high for most of the systems indicating an error(s) in the cross-section data or the theoretical methods. The uncertainties associated with the Monte Carlo results are 5 to 7 mk. As H/Pu decreases, the neutron spectrum becomes harder and non-thermal cross sections have a greater impact on reactivity. The reactivity effect of ^{240}Pu becomes greater as H/Pu decreases. There is no discernible trend with H/Pu ratio or with different percentages of ^{240}Pu . Thus, the results shown in Figure 16 do not suggest any particular cross section being in error. The six benchmarks listed in Table 26 were chosen to evaluate the effects of data changes.

EFFECT OF CHANGING ^{239}Pu DATA

Shown in Figure 17 are the ratios of k_{eff} values using the preliminary ^{239}Pu fit to k_{eff} values using ENDF/B-IV data. The new data give k_{eff} values which are 0.3 to 0.8% higher than the k_{eff} values calculated with ENDF/B-IV data, with the effect increasing as H/Pu ratio decreases. The changes in reaction rates in the vicinity of the 0.3 eV resonance are the major cause of the increase in k_{eff} . Broad group 20 is most important, followed by group 19. As H/Pu ratio decreases, the fraction of ^{239}Pu absorptions in the 0.3 eV resonance increases. As shown in Figure 8, η has increased by 2-3% around 0.3 eV. For Benchmark 2, 30% of the absorptions occur in groups 18, 19, and 20. For Benchmark 4, 14% of the absorptions occur in groups 18, 19, and 20; hence, the reactivity effect is much less.

The increase in η above 0.5 eV (Figure 8) does not affect the reactivity of the more thermal systems (high H/Pu). For low H/Pu systems k_{eff} is increased by 0.2%.

EFFECT OF CHANGING ^{240}Pu DATA

Shown in Figure 18 are the ratios of k_{eff} values using the new ^{240}Pu data to k_{eff} values using ENDF/B-IV data. For all systems the new data changes k_{eff} by less than 0.1%. The largest reactivity effects should be in systems with a low H/Pu ratio or systems with a high ^{240}Pu content. In Benchmark 2 (low H/Pu) only 8% of the absorptions occur in the vicinity of the 1 eV ^{240}Pu resonance. Thus, it would take at least a 12% increase in the resonance integral to effect a 1% decrease in k_{eff} . In Benchmark 14 (high ^{240}Pu) only 10% of the absorptions occur near the ^{240}Pu resonance.

EFFECT OF CHANGING THE H_2O KERNEL

The reactivity effect of replacing the modified Haywood kernel (ENDF) with a TISK kernel is shown in Figure 19 as the ratio of k_{eff} values. The reactivity effect is negative for Benchmark 2 (low H/Pu) and Benchmark 14 (high ^{240}Pu content). For the other systems the reactivity effect is positive. Shown in Figure 20 is the reactivity effect of going from the TISK kernel to the TISK-Koppel kernel. The changes are 0.2% at the most. As discussed earlier, the total cross section and the energy transfer matrix of hydrogen bound in water for the TISK kernel is quite different from the ENDF/B-IV kernel. Because of these differences one might expect to see differences in flux as a function of energy and/or space or a difference in the radial leakage. The differences between the TISK kernel and the TISK-Koppel kernel are not nearly as large.

The group fluxes for Benchmarks 2, 4, and 14 at the center of the system are shown in Tables 27, 28, and 29 respectively using the three kernels. They are normalized to the same fission source. In each case the flux at the high end of the thermal energy range is increased significantly. This is due to both the smaller total scattering cross section and less energy loss per scattering event. Increasing the flux tends to increase the radial leakage and hence, decrease k_{eff} . If the ^{240}Pu concentration is very high, k_{eff} would also decrease because of the increased absorption rate. For Benchmark 4 the increased absorption in the 1 eV ^{240}Pu resonance is worth -0.2% in going to the TISK kernel. For Benchmark 2 the effect is -0.4% and for Benchmark 14 it is -0.7%.

In going to the TISK-Koppel kernel, there is a very little change in the fluxes for groups 13-17. Therefore, the reactivity effect is small.

The second area of interest is in groups 19-21 which encompass the 0.3 eV resonance of ^{239}Pu . If the flux increases in these groups, k_{eff} will decrease because of the lower value of η compared to the rest of the thermal energy range. In all cases the flux does increase; however, not enough to affect the reactivity significantly.

The flux in group 25 obtained with the TISK kernel is significantly lower for all three systems. The TISK kernel scatters only half as many neutrons from group 24 to group 25 as the ENDF kernel.

The last area of interest is the radial leakage. Shown in Table 30 is the difference in radial leakage from the fissile region in going to the TISK kernel expressed as percentage of total neutrons absorbed in the system and leaking from the system. For reflected systems this is the difference between leakage out and leakage into the fission region. For all systems the leakage is reduced which leads to an increase in reactivity. Benchmark 14 has much less leakage than the other systems; hence, the change in leakage is worth less in terms of reactivity.

Although small, all systems exhibit a reduction in the fast-energy neutron leakage. This is due to a change in the spatial fission rate, most of which is in the bottom 6 groups. The TISK kernel has led to a flux distribution which is reduced at the edge of the fissile region.

The leakage in group 13, the top of the thermal calculation, increases appreciably for the unreflected systems. This could be due to the increase in flux as shown in Tables 27-29. However, the flux is also increased in groups 14-17 with no increase in leakage. In group 18 neutron leakage is decreased significantly yet the flux is increased 5-7%. In groups 21-23 (0.225 to 0.030 eV) the neutron leakage is decreased significantly for Benchmarks 4 and 7 but not for the other systems.

In going from the TISK kernel to the TISK-Koppel kernel there is very little change in leakage. The reactivity worth is less than 0.1%.

For the kernels used in this study, two parameters were sensitive to the type of kernel. Absorption in the ^{240}Pu resonance was increased and leakage from the system was decreased in the going to the TISK kernel. For the benchmarks considered in this study the effects were of the same order of magnitude. The leakage effect ranged from +0.1 to +0.7% in reactivity. The ^{240}Pu absorption effect ranged from -0.2 to -1.0% in reactivity. For other systems one or the other may dominate.

996 125

CONCLUSIONS AND RECOMMENDATIONS

Neutronics analyses of critical systems were performed to identify where certain cross sections may be deficient. The integral reactivity parameter, k_{eff} , was used to make judgements about the cross sections. The cross sections of interest are stainless steel, ^{239}Pu thermal, ^{240}Pu resonance (1 eV), and scattering of hydrogen bound in water.

A limited number of experiments were available to evaluate stainless-steel data. The calculation of these experiments led to conflicting conclusions concerning biases. Other uncertainties or biases in the experiments and/or calculations were concluded to be large enough to preclude the determination of biases in the cross-section data. For the systems used in this study, uncertainties in k_{eff} due to uncertainties in the elemental cross sections are small compared to the other calculational biases and uncertainties. Although this study cannot demonstrate a need to improve the cross-section data for the elements of stainless steel, it would be desirable to design and perform benchmark experiments more appropriate for the evaluation of stainless-steel cross-section data.

Results of a preliminary fit of ^{239}Pu data were used to calculate plutonium benchmarks. Calculated values of k_{eff} for several homogeneous plutonium benchmarks were compared with values obtained with ENDF/B-IV data. The new data resulted in k_{eff} values which ranged from 0.3 to 0.8% higher than the values calculated with ENDF/B-IV data. The primary cause of the increase is due to reactions in the 0.3 eV resonance. The production-to-absorption ratio, $\eta = \nu\sigma_f/\sigma_a$, is higher for the new data. Uncertainties in 2200 m/s ENDF/B-IV data lead to small uncertainties in k_{eff} . No uncertainties have been generated for the new cross-section data. However, the ^{239}Pu data is known least accurately in the vicinity of the 0.3 eV resonance. Consequently, a good measurement of the data between 0.0 and 0.5 eV should be performed.

A least squares fit of ^{240}Pu data from 0 to 3 eV was performed to obtain a best estimate of the cross section. The new fit resulted in a resonance integral which is 1.9% larger than ENDF/B-IV data. This small change had a negligible effect on k_{eff} ($\leq 0.1\%$) for the plutonium systems considered in

this study. Since the cross-section uncertainty is $\sim 2\%$, there is not a need to improve the accuracy of the data. Uncertainties (or errors) in the theoretical methods used to calculate ^{240}Pu reaction rates are much larger than uncertainties due to the cross-section data.

Two kernels for hydrogen bound in water were generated. Reactivity calculations for several plutonium benchmarks using these two kernels were compared to calculations using the ENDF kernel (modified Haywood). The first kernel was generated with TISK assuming isotropic scattering. Three major differences between the ENDF and TISK kernels are apparent. First, the scattering from TISK is more peaked, thus the spectrum is harder. Hence, the flux in the vicinity of 1 eV was increased by $\sim 10\%$. A second difference between the TISK and ENDF kernels is the low total scattering cross section generated by TISK between 1 and 3 eV. The third difference between the kernels is the higher total scattering cross section generated by TISK below 0.0253 eV. The increased cross section at low energies has a positive effect on k_{eff} because it decreases neutron leakage from the systems. The increased absorption rate in ^{240}Pu is worth -0.2 to -0.7% in reactivity for the plutonium benchmarks considered. The reduced neutron leakage is worth $+0.1$ to $+0.6\%$ in reactivity for the plutonium benchmarks considered. The magnitudes of these effects suggest that the model for neutron thermalization could be causing a significant error in the calculated reactivity of plutonium systems. The TISK kernel generated for this study needs to be refined because of the total cross section mismatch between it and the ENDF kernel. The results obtained in this study indicate that kernel effects can have a significant impact on calculated reactivity values for plutonium systems. Thus, a thorough evaluation of neutron scattering in water is recommended.

A second kernel (TISK-Koppel) was generated with TISK by modifying the code to include anisotropic scattering. It is substantially different from the kernel generated assuming isotropic scattering. However, reactivity results obtained using the TISK-Koppel kernel were essentially the same as those using the TISK kernel. The reactivity changes are of the order of 0.1% . However, for geometrically more complex systems, anisotropic scattering could be very important. Further, comparisons should be performed for systems of fuel rods in water to determine if the anisotropic effect is significant.

REFERENCES

1. U. P. Jenquin and S. R. Bierman, "Benchmark Experiments to Test Plutonium and Stainless Steel Cross Sections," NUREG/CR-210, PNL-2273, Pacific Northwest Laboratory, June 1978.
2. N. M. Greene et. al., "AMPX: A Modular Code System for Generating Coupled Multigroup Neutron - Gamma Libraries from ENDF/B," ORNL/TM-3706, Oak Ridge National Laboratory, March 1976.
3. W. E. Ford, III, C. C. Webster, and R. M. Westfall, "A 218-Group Neutron Cross-Section Library in the AMPX Master Interface Format for Criticality Safety Studies," ORNL/CSD-TM-4, Oak Ridge National Laboratory, July 1976.
4. L. W. Nordheim, "The Theory of Resonance Absorption," Proceedings of Symposia in Applied Mathematics, Vol. XI, p. 58, Garrett Birkhoff and Eugene P. Wigner, Eds., Am. Math. Soc. (1961).
5. J. K. Thompson, "Nonlinear Model Fitting of Thermal Neutron Data and Its Application in Resonance Parameter Uncertainty Analysis", Proceedings of a Seminar-Workshop: A Review of the Theory and Application of Sensitivity and Uncertainty Analysis, ORNL/RSIC-42, Oak Ridge National Laboratory, February 1979.
6. L. W. Weston and J. H. Todd, "Neutron Capture Cross Section of Plutonium-240," NSE 63, 143 (1977).
7. B. R. Leonard, Jr., E. J. Seppi, and W. J. Friesen, "The Width of the 1 eV Resonance in Plutonium-240," NSE 5, 32 (1959).
8. R. C. Block, G. G. Slaughter, and J. A. Harvey, "Thermal Neutron Cross Section Measurements of ^{233}U , ^{235}U , ^{240}Pu , ^{234}U , and ^{129}I with the ORNL Fast Chopper Time-of-Flight Neutron Spectrometer," NSE 8, 112 (1960).
9. M. Lounsbury, R. W. Durham, and G. C. Hanna, Proc. Conf. on Nuclear Data for Reactors, Helsinki, IAEA, 1, 287 (1970).
10. G. H. Lander and M. H. Mueller, "Coherent Scattering Amplitude of ^{240}Pu and ^{242}Pu ," Acta Crystallographica/B, 27, 2284, November 1971.
11. B. R. Leonard, Jr., E. J. Seppi, W. J. Friesen and E. M. Kinderman, "The Slow Neutron Fission Cross Section of ^{240}Pu ," Bull. Am. Phys. Soc. II, 1, 248 (1956) and B. R. Leonard, Jr., and R. H. Odegarden, USAEC Report HW-67219 (1960).
12. A. H. Jaffey et. al., "Half-Life of ^{239}Pu by Two Independent Methods," Phys. Rev. C16, 354-369, (1977).

13. R. Gwin, R. R. Spencer, R. W. Ingle, J. H. Todd, and H. Weaver, "Measurements of the Average Number of Prompt Neutrons Emitted per Fission of ^{239}Pu and ^{235}U ," ORNL/TM-6246, Oak Ridge National Laboratory, May 1978.
14. S. Weinstein, R. Reed, and R. C. Block, "Neutron Multiplicity Measurements for U-233, U-235, and Pu-239 Resonance Fission," IAEA-SM-122/113.
15. R. W. Hockenbury, Private Communication to B. R. Leonard, Jr. (August 23, 1973).
16. H. C. Honeck and D. R. Finch, "FLANGE II (Version 71-1) A Code to Process Thermal Neutron Data from an ENDF/b Tape," DP-1278, Savannah River Laboratory, 1971.
17. A. G. Gibbs and C. W. Lindenmeier, "TISK: A Program for Calculating Thermal Neutron Scattering Kernels, and Its Application to H_2O ," BNWL-1675, Battelle, Pacific Northwest Laboratory, June 1972.
18. P. A. Egelstaff and P. Schofield, "On the Evaluation of the Thermal Neutron Scattering Law," NSE 12, 260-270 (1972).
19. J. W. Cooley and J. W. Tukey, "An Algorithm for the Machine Calculation of Complex Fourier Series," Math. Comput., 19, 297 (1965).
20. J. U. Koppel and J. A. Young, "Neutron Scattering by Water Taking into Account the Anisotropy of the Molecular Vibrations," NSE 19, 412-417, (1964).
21. A. H. Stroud, "Appropriate Calculation of Multiple Integrals," Prentice-Hall, Englewood Cliffs, N.J., pp. 359-361, 1971.
22. O.K. Harling, "Slow Neutron Inelastic Scattering Study of Light Water and Ice," Journal of Chemical Physics, 50, No. 12; 5279-5296 (1969).
23. B. C. Haywood, "The Spectral Density of Hydrogen in Water," Journal of Nuclear Energy, 21, 249-262, (1967).
24. B. H. Duane, "Maximum Likelihood Nonlinear Correlated Fields," BNWL-390, Pacific Northwest Laboratory, (1967).
25. J. U. Koppel and D. H. Houston, "Reference Manual for ENDF Thermal Neutron Scattering Data, GA-8774 (1968).
26. J. U. Koppel et. al., "A Unified Code for Thermal Neutron Scattering," GA-7417 (1967).
27. S. F. Mughabghab and D. I. Garber, "Neutron Cross Sections Volume I, Resonance Parameters", BNL-325 (3rd Ed.), Brookhaven National Laboratory, June 1973.

996 127

TABLE 1. 25 Broad-Group Structure

Gp. No.	Energy Range, eV		ΔU
	Upper	Lower	
1	2.0 +7*	3.0 +6	1.89712
2	3.0 +6	1.4 +6	0.76214
3	1.4 +6	9.0 +5	0.44183
4	9.0 +5	4.0 +5	0.81093
5	4.0 +5	1.0 +5	1.38629
6	1.0 +5	1.7 +4	1.77196
7	1.7 +4	3.0 +3	1.73460
8	3.0 +3	5.5 +2	1.69645
9	5.5 +2	1.0 +2	1.70475
10	1.0 +2	30	1.20397
11	30	10	1.09861
12	10	3.05	1.18744
13	3.05	1.77	0.54417
14	1.77	1.30	0.30861
15	1.30	1.13	0.14015
16	1.13	1.00	0.12222
17	1.00	0.80	0.22314
18	0.80	0.40	0.69315
19	0.40	0.325	0.20764
20	0.325	0.225	0.36772
21	0.225	0.100	0.81093
22	0.100	0.050	0.69315
23	0.050	0.030	0.51082
24	0.030	0.010	1.09862
25	0.010	1. -5	6.90775

*Read as 2.0×10^7

996 130

TABLE 2. Homogeneous Plutonium Benchmarks

No.	H/Pu Atom Ratio	% ^{240}Pu	Pu Density, g/cm^3	Geometry
1	3695	0	0.007	Infinite
2*	125	5	0.172	Sphere
3*	980	1	0.026	Sphere
4*	758	5	0.034	Sphere
5	15	2	1.12	Parallelepiped
6	0	5	15.6	Sphere
7*	422	5	0.058	Slab
8	910	14	0.028	Cylinder
9	50	18	0.37	Parallelepiped
10	210	8	0.116	Cylinder
11	0	18	5.8	Parallelepiped
12	5	11	2.3	Parallelepiped
13	0	20	15.7	Sphere
14*	623	43	0.041	Cylinder
15a*	1067	5	0.024	Sphere
15b	1031	5	0.025	Sphere

TABLE 3. Fundamental Theoretical Forms

Modified Adler-Adler Formalism

$$\sigma_x(E)\sqrt{E} = \frac{\pi\hbar^2}{2M_n} \left[\sum_{r=1}^{NR} \frac{g_r \Gamma_{nr}^0 \Gamma_{xr} + A_{xr}(E-E_r)}{(E-E_r)^2 + (\Gamma_r(E)/2)^2} + \sum_{b=1}^{NB} B_{xb} E^{b-1} \right]$$

$$x = \gamma, f$$

Multi-Level Breit-Wigner Formalism

$$\sigma_{\text{coh}}(E)/4\pi = [g_+ b_+(E) + g_- b_-(E)]^2 + [g_+ d_+(E) + g_- d_-(E)]^2$$

$$\sigma_{\text{inc}}(E)/4\pi = g_+ g_- [(b_+(E) - b_-(E))^2 + (d_+(E) - d_-(E))^2]$$

$$\sigma_s(E)/4\pi = g_+^2 [b_+^2(E) + d_+^2(E)] + g_-^2 [b_-^2(E) + d_-^2(E)]$$

$$b_{\pm}(E) = R + \frac{\hbar}{\sqrt{8M_n}} \sum_{r=\pm} \frac{\Gamma_{nr}^0 (E-E_r)}{(E-E_r)^2 + (\Gamma_r(E)/2)^2}$$

$$d_{\pm}(E) = \frac{\hbar}{\sqrt{32M_n}} \sum_{r=\pm} \frac{\Gamma_{nr}^0 \Gamma_r}{(E-E_r)^2 + (\Gamma_r(E)/2)^2}$$

Spin-Dependent Resonance Formalism

$$v(E)\sigma_f(E)\sqrt{E} = v_+ \sigma_f^+(E)\sqrt{E} + v_- \sigma_f^-(E)\sqrt{E} + v_b \sigma_f^b(E)\sqrt{E}$$

$$\sigma_f^{\pm}(E)\sqrt{E} = \frac{\pi\hbar^2}{2M_n} \sum_{r=\pm} \frac{g_r \Gamma_{nr}^0 \Gamma_{fr} + A_{fr}(E-E_r)}{(E-E_r)^2 + (\Gamma_r(E)/2)^2}$$

$$\sigma_f^b(E)\sqrt{E} = \frac{\pi\hbar^2}{2M_n} \sum_{b=1}^{NB} B_{fb} E^{b-1}$$

$$v_b = \lambda v_+ + (1-\lambda)v_-$$

NOTE: For all forms $\Gamma_r(E) = \Gamma_{fr} + \Gamma_{\gamma r} + \Gamma_{nr}^0 \sqrt{E}$

TABLE 4. Combinations of Fundamental Theoretical Forms

Absorption

$$\sigma_a(E)\sqrt{E} = \sigma_f(E)\sqrt{E} + \sigma_y(E)\sqrt{E}$$

Total

$$\sigma_t(E)\sqrt{E} = \sigma_a(E)\sqrt{E} + \sigma_s(E)\sqrt{E}$$

Alpha

$$\alpha(E) = \sigma_y(E)\sqrt{E}/\sigma_f(E)\sqrt{E}$$

Eta

$$\eta(E) = (\nu(E)\sigma_f(E)\sqrt{E})/\sigma_a(E)\sqrt{E}$$

Nu

$$\nu(E) = (\nu(E)\sigma_f(E)\sqrt{E})/\sigma_f(E)\sqrt{E}$$

Sums*

$$S(E) = \lambda\sigma_x^z(E) + (1-\lambda)\sigma_x^{z'}(E) \quad (\text{possibly with } \sqrt{E} \text{ multiplier})$$

Ratios*

$$R(E) = \sigma_x^z(E)/\sigma_x^{z'}(E) \quad (\text{possibly with } \sqrt{E} \text{ cancelling})$$

*Sums and ratios may be formed with any theory form x for isotope z and any theory form x' for isotope z', except η and ν .

996 133

TABLE 5. The Parameters of the Model

Theory Parameters for Each Isotope

<u>Resonance Parameters</u>		<u>Non-Resonance Parameters</u>	
E_r	Resonance Energy (eV)	$B_{f1}, B_{f2}^*, B_{f3}^*$	Coefficients of background, polynomials and fission and capture
Γ_{nr}^o	Reduced Neutron width (eV ^{1/2})	$B_{\gamma 1}, B_{\gamma 2}^*, B_{\gamma 3}^*$	
Γ_{fr}	Fission width (eV)	R	Potential scattering radius (b ^{1/2})
$\Gamma_{\gamma r}$	Capture width (eV)	ν_+, ν_-, ν_b	Neutrons per fission in parallel-, anti-parallel-, and non-resonance fission respectively
A_{fr}	Fission asymmetry coefficient (eV ^{1/2})		
$A_{\gamma r}$	Capture asymmetry coefficient (eV ^{1/2})		
(g_r)	Input constant - statistical weight factor)		

Experimental Parameters

N_s^*	Normalization factor for sth data set
α_s^*, β_s^*	Energy-scale adjustment parameters for sth data set
	$E = E_m (\alpha_s + \beta_s \sqrt{E_m})$
λ_s^*	Composition parameter for sth data set, if applicable

* Indicates that parameter does not have to be present

TABLE 6. Absolute Data for ^{240}Pu Used for Normalization

<u>Cross Section</u>	<u>Datum</u>	<u>Fitted Value</u>
$\sigma_{\gamma}(.0253)$	$289.5 \pm 1.4\text{b}$	$289.41 \pm 1.63\text{b}$
$\sigma_{\text{S}}(.08)$	$1.54 \pm .05\text{b}$	$1.537 \pm .059\text{b}$
σ_{f} PEAK	$33 \pm 3\text{b}$	$33.00 \pm 3.55\text{b}$

TABLE 7. Preliminary Results of ^{240}Pu Data Analysis

<u>2200 m/s Cross Sections</u>	<u>1 eV Resonance Parameters</u>
$\sigma_{\text{t}}^{\circ} = 291.3 \pm 1.64\text{b}$	$E_0 = 1.0594 \pm .008 \text{ eV}$
$\sigma_{\gamma}^{\circ} = 289.4 \pm 1.63\text{b}$	$\Gamma_{\text{n}}^{\circ} = 2.451 \pm .0026 \text{ meV/eV}^{1/2}$
$\sigma_{\text{S}}^{\circ} = 1.813 \pm .060\text{b}$	$\Gamma_{\gamma} = 29.72 \pm .41 \text{ meV}$
	$\Gamma_{\text{f}} = 5.76 \pm .60 \text{ } \mu\text{eV}$

1/V Capture Background at Thermal is $10.4 \pm 2.1\text{b}$

Fitted ^{239}Pu σ_{γ} impurity in Weston and Todd data ($.82 \pm .09\%$)

TABLE 8. Resonance Parameters from the Preliminary Fit of ^{239}Pu Data

<u>Parameter</u>	<u>Bound Level</u>	<u>Visible Level</u>
E_0 (eV)	-0.071876	.29687
Γ_n^0 ($\mu\text{eV}/\sqrt{\text{eV}}$)	48.963	149.46
Γ_γ (meV)	38.892	39.508
Γ_f (meV)	405.75	59.990
A_f ($\mu\text{eV}/\sqrt{\text{eV}}$)	2.2702	5.8061

TABLE 9. 2200 m/s Parameters for ^{239}Pu

<u>Parameter</u>	<u>ENDF/B-IV</u>	<u>Preliminary New Data</u>
σ_t	1019.9	1027.1
σ_c	270.2	271.5
σ_f	741.7	748.5
v_t	2.8733	2.8766
α	0.3643	0.3627
η	2.1061	2.1109

096 136

TABLE 10. Parameters for the Six Peaks of the Phonon Spectrum

<u>Peak</u>	<u>γ_i</u>	<u>δ_i</u>	<u>F_i</u>
1	0.1647	0.1941	0.0279
2	0.8794	0.2216	0.0105
3	2.1629	0.6402	0.3401
4	2.6258	0.1814	0.1905
5	7.9479	0.2597	0.1099
6	17.4520	0.6903	0.3206

996 137

TABLE 11. Comparison of H₂O Kernels for Broad Group 13

<u>FINAL GP. NO.</u>	<u>ENDF</u>	<u>TISK</u>	<u>TISK-Koppel</u>
13	5.750	5.420	5.559
14	4.098	3.656	3.791
15	1.485	1.253	1.337
16	1.133	0.934	1.000
17	1.739	1.412	1.516
18	3.464	2.860	2.823
19	0.645	0.546	0.487
20	0.852	0.725	0.621
21	1.039	0.861	0.705
22	0.387	0.289	0.232
23	0.145	0.093	0.075
24	0.117	0.070	0.057
25	0.035	0.018	0.015
TOTAL	20.889	18.139	18.216

TABLE 12. Comparison of H₂O Kernels for Broad Group 14

<u>FINAL GP. NO.</u>	<u>ENDF</u>	<u>TISK</u>	<u>TISK-Koppel</u>
13	0.007	0.006	0.006
14	4.195	4.353	4.506
15	2.313	2.201	2.123
16	1.695	1.591	1.571
17	2.625	2.400	2.476
18	5.294	4.591	4.875
19	0.982	0.817	0.925
20	1.287	1.058	1.196
21	1.492	1.211	1.351
22	0.487	0.393	0.442
23	0.154	0.124	0.142
24	0.110	0.091	0.106
25	0.030	0.024	0.028
TOTAL	20.670	18.860	19.748

TABLE 13. Comparison of H₂O Kernels for Broad Group 15

<u>FINAL GP. NO.</u>	<u>ENDF</u>	<u>TISK</u>	<u>TISK-Koppel</u>
14	0.052	0.047	0.050
15	2.837	3.161	3.462
16	2.437	2.313	2.240
17	3.254	3.119	2.825
18	6.549	5.987	6.196
19	1.230	1.081	1.082
20	1.615	1.396	1.490
21	1.875	1.595	1.786
22	0.612	0.514	0.591
23	0.0193	0.162	0.190
24	0.0138	0.119	0.143
25	0.037	0.031	0.037
TOTAL	20.828	19.525	20.093

TABLE 14. Comparison of H₂O Kernels for Broad Group 16

<u>FINAL GP. NO.</u>	<u>ENDF</u>	<u>TISK</u>	<u>TISK-Koppel</u>
15	0.123	0.106	0.118
16	2.873	3.156	3.480
17	4.208	4.002	3.833
18	7.342	6.881	6.908
19	1.403	1.267	1.255
20	1.845	1.646	1.597
21	2.148	1.877	1.937
22	0.701	0.606	0.679
23	0.221	0.191	0.221
24	0.157	0.140	0.165
25	0.042	0.036	0.043
TOTAL	21.063	19.910	20.236

TABLE 15. Comparison of H₂O Kernels for Broad Group 17

<u>FINAL GP. NO.</u>	<u>ENDF</u>	<u>TISK</u>	<u>TISK-Koppell</u>
16	0.081	0.070	0.078
17	4.354	4.586	5.002
18	9.124	8.704	8.268
19	1.647	1.525	1.659
20	2.190	1.995	2.072
21	2.553	2.313	2.265
22	0.854	0.748	0.747
23	0.261	0.235	0.244
24	0.185	0.172	0.184
25	0.049	0.044	0.049
TOTAL	21.278	20.392	20.567

TABLE 16. Comparison of H₂O Kernels for Broad Group 18

<u>FINAL GP. NO.</u>	<u>ENDF</u>	<u>TISK</u>	<u>TISK-Koppell</u>
17	0.028	0.026	0.027
18	9.613	9.754	10.250
19	2.942	2.807	2.680
20	3.541	3.472	3.216
21	4.105	3.905	3.674
22	1.304	1.233	1.233
23	0.402	0.382	0.403
24	0.279	0.276	0.302
25	0.073	0.070	0.080
TOTAL	22.387	21.925	21.865

TABLE 17. Comparison of H₂O Kernels for Broad Group 19

<u>FINAL GP. NO.</u>	<u>ENDF</u>	<u>TISK</u>	<u>TISK-Koppel</u>
18	0.437	0.383	0.416
19	6.913	7.425	8.285
20	6.748	6.392	6.447
21	7.046	6.736	6.009
22	2.174	2.080	1.787
23	0.649	0.619	0.542
24	0.435	0.432	0.390
25	0.110	0.107	0.100
TOTAL	24.511	24.174	23.976

TABLE 18. Comparison of H₂O Kernels for Broad Group 20

<u>FINAL GP. NO.</u>	<u>ENDF</u>	<u>TISK</u>	<u>TISK-Koppel</u>
18	0.019	0.017	0.016
19	0.457	0.401	0.441
20	10.238	10.830	11.962
21	10.503	9.952	9.542
22	3.179	3.004	2.660
23	0.976	0.922	0.823
24	0.656	0.643	0.581
25	0.165	0.157	0.144
TOTAL	26.192	25.927	26.168

996 141

TABLE 19. Comparison of H₂O Kernels for Broad Group 21

<u>FINAL GP. NO.</u>	<u>ENDF</u>	<u>TISK</u>	<u>TISK-Koppel</u>
19	0.007	0.006	0.006
20	0.453	0.402	0.424
21	18.808	19.967	21.375
22	7.599	6.751	6.546
23	2.092	2.042	1.841
24	1.345	1.318	1.204
25	0.324	0.292	0.273
TOTAL	30.629	30.778	31.669

TABLE 20. Comparison of H₂O Kernels for Broad Group 22

<u>FINAL GP. NO.</u>	<u>ENDF</u>	<u>TISK</u>	<u>TISK-Koppel</u>
20	0.015	0.013	0.012
21	2.673	2.250	2.239
22	25.086	28.560	29.852
23	6.938	5.187	5.307
24	2.669	2.496	2.365
25	0.631	0.650	0.606
TOTAL	38.013	39.156	40.381

996 142

TABLE 21. Comparison of H₂O Kernels for Broad Group 23

<u>FINAL GP. NO.</u>	<u>ENDF</u>	<u>TISK</u>	<u>TISK-Koppel</u>
21	0.909	0.873	0.787
22	8.657	6.424	6.573
23	26.898	34.864	35.621
24	9.063	6.127	6.250
25	0.723	0.637	0.626
TOTAL	46.257	48.930	49.862

TABLE 22. Comparison of H₂O Kernels for Broad Group 24

<u>FINAL GP. NO.</u>	<u>ENDF</u>	<u>TISK</u>	<u>TISK-Koppel</u>
21	0.554	0.509	0.463
22	3.183	2.847	2.698
23	8.625	5.667	5.781
24	40.852	53.238	53.744
25	5.746	2.141	2.155
TOTAL	58.963	64.405	64.845

TABLE 23. Comparison of H₂O Kernels for Broad Group 25

<u>FINAL GP. NO.</u>	<u>ENDF</u>	<u>TISK</u>	<u>TISK-Koppel</u>
21	0.557	0.467	0.437
22	3.197	3.215	2.993
23	2.931	2.543	2.499
24	24.332	9.322	9.383
25	48.074	97.537	97.922
TOTAL	79.095	113.087	113.238

TABLE 24. Evaluation of Stainless Steel Using Homogeneous Plutonium Benchmarks

<u>Parameter</u>	<u>15a</u>	<u>15b</u>
SS Thickness, cm	0.122	0.325
Pu Density, g/cm ³	0.0244	0.0252
H/Pu Atom Ratio	1067	1031
k _∞	1.4895	1.4995
SS Absorptions	0.0225	0.0466
k _{eff}	1.0207	1.0187

TABLE 25. Evaluation of Stainless Steel Using Enriched UO₂ Lattice Benchmarks

<u>Parameter</u>	<u>42a</u>	<u>42b</u>
Clad Material	SS	Al
k _∞	1.1777	1.2941
Clad Absorptions	0.0733	0.0047
k _{eff}	0.9973	0.9917
Critical Number of Rods	1766	950
Leakage Fraction	0.153	0.234

006 144

TABLE 26. Description of Benchmarks Used to Evaluate Data Changes

Benchmark No.	H/Pu	% ^{240}Pu	Pu Density, g/cm^3	Geometry	Radius or Thickness, cm
2	125	4.5	0.172	Sphere	19.32
3	980	0.5	0.026	Sphere*	17.78
4	758	4.5	0.034	Sphere	19.32
7	422	4.6	0.058	Slab	16.91
14	623	42.9	0.041	Cylinder*	30.51
15a	1067	4.5	0.024	Sphere*	19.32

*Reflected with H_2O ; other systems are unreflected.

TABLE 27. Group Fluxes for Benchmark 2 Using Various Water Kernels

Gp. No.	ENDF	TISK	% Difference	TISK-Koppel	% Difference
13	22.033	25.982	+17.9	26.098	+0.4
14	12.587	14.620	+16.2	14.232	-2.7
15	5.514	6.228	+13.0	6.149	-1.3
16	2.543	2.732	+ 7.4	2.736	+0.1
17	7.943	8.597	+ 8.2	8.731	+1.6
18	24.788	26.114	+ 5.4	27.128	+3.9
19	4.315	4.431	+ 2.7	4.599	+3.8
20	4.836	4.881	+ 0.9	4.951	+1.4
21	18.277	18.468	+ 1.0	18.448	-0.1
22	19.254	19.079	- 0.9	18.689	-2.0
23	10.853	10.498	- 3.3	10.236	-2.5
24	8.816	8.549	- 3.0	8.309	-2.8
25	1.729	1.511	-12.6	1.467	-2.9

TABLE 28. Group Fluxes for Benchmark 4 Using Various Water Kernels

<u>Gp. No.</u>	<u>ENDF</u>	<u>TISK</u>	<u>% Difference</u>	<u>TISK-Koppel</u>	<u>% Difference</u>
13	21.248	25.213	+18.7	25.318	+0.4
14	12.312	14.370	+16.7	13.955	-2.9
15	5.625	6.398	+13.7	6.310	-1.4
16	4.260	4.718	+10.8	4.722	+0.1
17	8.941	9.812	+ 9.7	9.949	+1.4
18	29.527	31.561	+ 6.9	32.957	+4.4
19	8.126	8.563	+ 5.4	9.136	+6.7
20	14.023	14.540	+ 3.7	15.343	+5.5
21	70.820	71.568	+ 1.1	72.615	+1.5
22	130.978	131.998	+ 0.8	130.319	-1.3
23	94.240	94.358	+ 0.1	92.963	-1.5
24	91.974	93.851	+ 2.0	92.280	-1.7
25	20.558	19.717	- 4.1	19.354	-1.9

TABLE 29. Group Fluxes for Benchmark 14 Using Various Water Kernels

<u>Gp. No.</u>	<u>ENDF</u>	<u>TISK</u>	<u>% Difference</u>	<u>TISK-Koppel</u>	<u>% Difference</u>
13	21.199	25.147	+18.6	25.291	+0.6
14	12.278	14.305	+16.5	13.917	-2.7
15	5.196	5.859	+12.8	5.791	-1.2
16	1.664	1.765	+ 6.1	1.770	+0.3
17	7.303	7.880	+ 7.9	8.024	+1.8
18	26.722	28.209	+ 5.6	29.552	+4.8
19	7.831	8.171	+ 4.3	8.770	+7.3
20	14.445	14.840	+ 2.7	15.810	+6.5
21	74.823	74.467	- 0.5	75.917	+1.9
22	142.78	141.80	- 0.7	140.61	-0.8
23	103.61	102.32	- 1.2	101.26	-1.0
24	101.61	102.33	+ 0.7	101.08	-1.2
25	22.756	21.563	- 5.2	21.261	-1.4

996 147

TABLE 30. Reactivity Effect of Water Kernel on Leakage

<u>Gp. No.</u>	<u>No Reflector</u>			<u>Reflected</u>		
	<u>2</u>	<u>4</u>	<u>7</u>	<u>3</u>	<u>14</u>	<u>15a</u>
1	+0.02	+0.02	+0.01	+0.03	+0.02	+0.02
2	+0.02	+0.03	+0.02	+0.04	+0.03	+0.04
3	+0.01	+0.01	+0.01	+0.02	+0.01	+0.02
4	+0.01	+0.01	+0.01	+0.02	+0.01	+0.02
5	+0.01	+0.01	+0.01	+0.02	+0.01	+0.02
6	0	+0.01	0	+0.01	+0.01	+0.01
7	0	0	0	0	0	0
8	0	0	0	0	0	0
9	0	0	0	0	0	0
10	0	0	0	0	0	0
11	0	0	0	0	0	0
12	0	0	0	0	0	0
13	-.04	-.05	-.05	-.02	0	-.02
14	0	-.01	0	+0.02	+0.01	+0.02
15	+0.01	0	+0.01	+0.01	+0.01	+0.01
16	+0.01	0	+0.01	+0.02	+0.01	+0.02
17	+0.01	+0.01	+0.02	+0.03	+0.01	+0.03
18	+0.07	+0.06	+0.10	+0.12	+0.03	+0.11
19	+0.01	+0.02	+0.03	+0.03	+0.01	+0.03
20	+0.01	+0.03	+0.04	+0.04	+0.01	+0.04
21	+0.03	+0.12	+0.10	+0.02	-.02	+0.02
22	+0.03	+0.16	+0.11	-.02	-.04	-.01
23	+0.01	+0.10	+0.06	-.01	-.02	0
24	+0.01	+0.07	+0.04	+0.02	0	+0.02
25	0	+0.03	+0.01	0	0	0
Total	+0.23	+0.63	+0.54	+0.40	+0.10	+0.40

POOR ORIGINAL

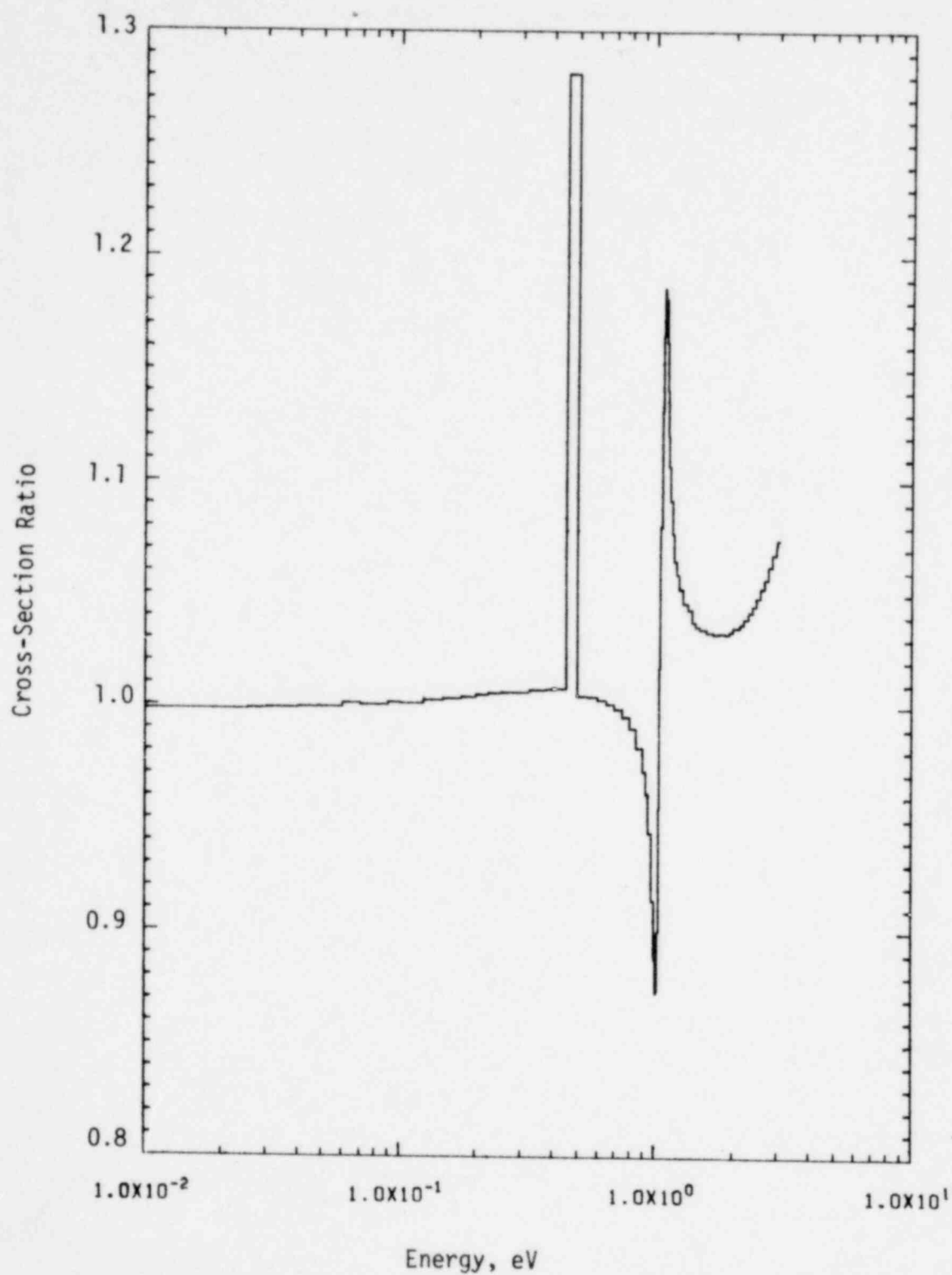


FIGURE 1. Ratio of New ^{240}Pu Data to ENDF/B-IV ^{240}Pu Data

POOR ORIGINAL

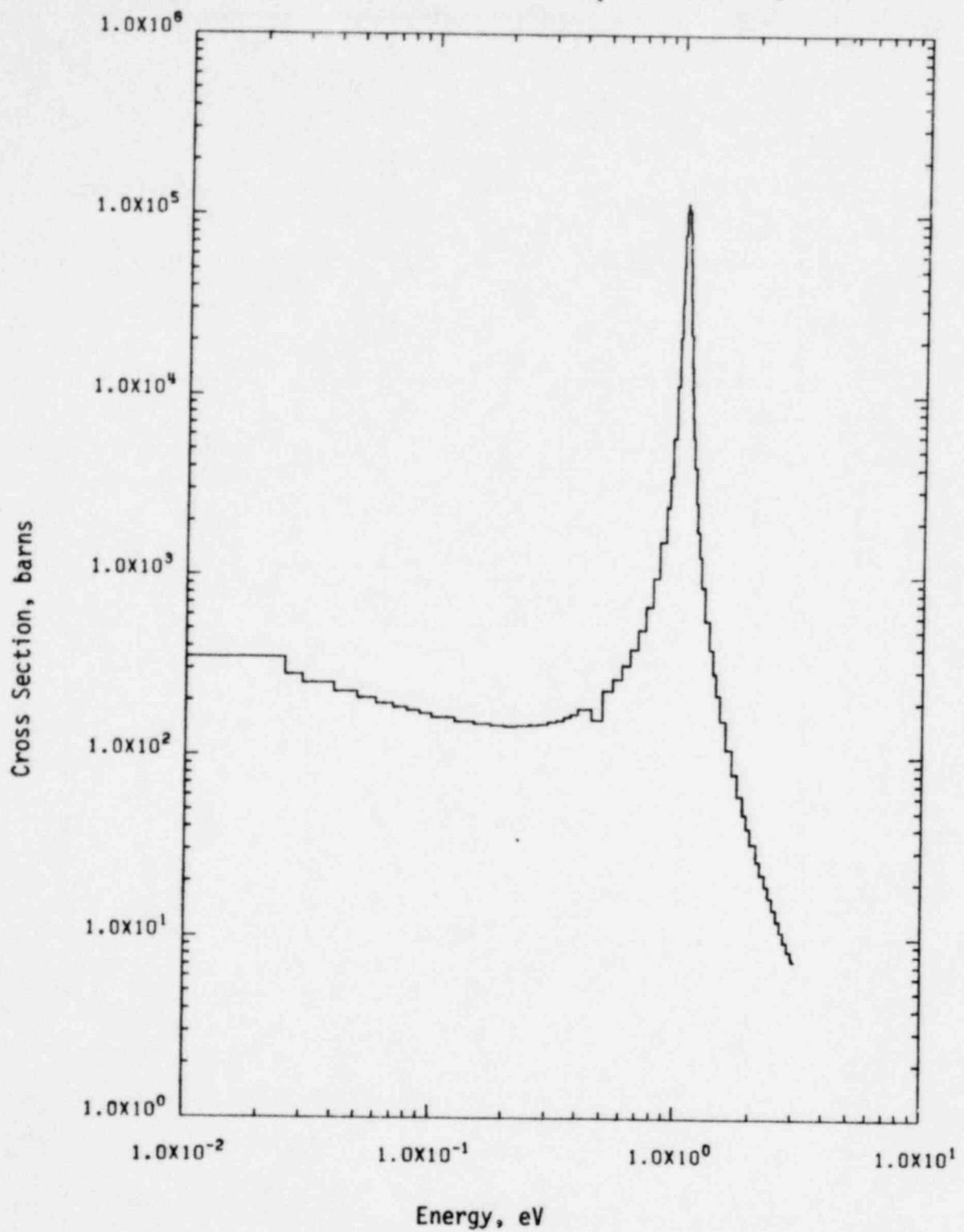


FIGURE 2. ENDF/B-IV Capture data for ^{240}Pu

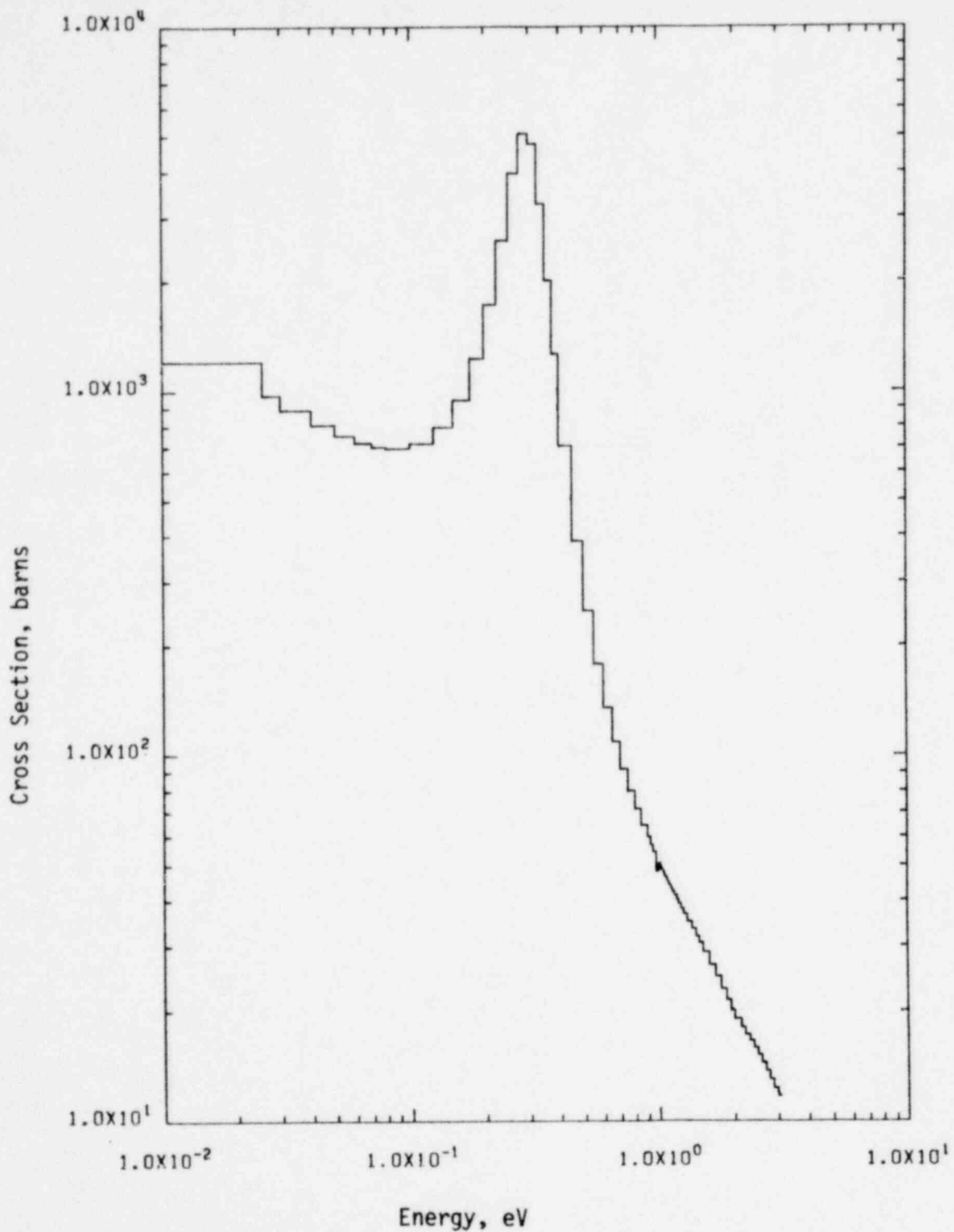


FIGURE 3. ENDF/B-IV Absorption Cross Section for ^{239}Pu

POOR ORIGINAL

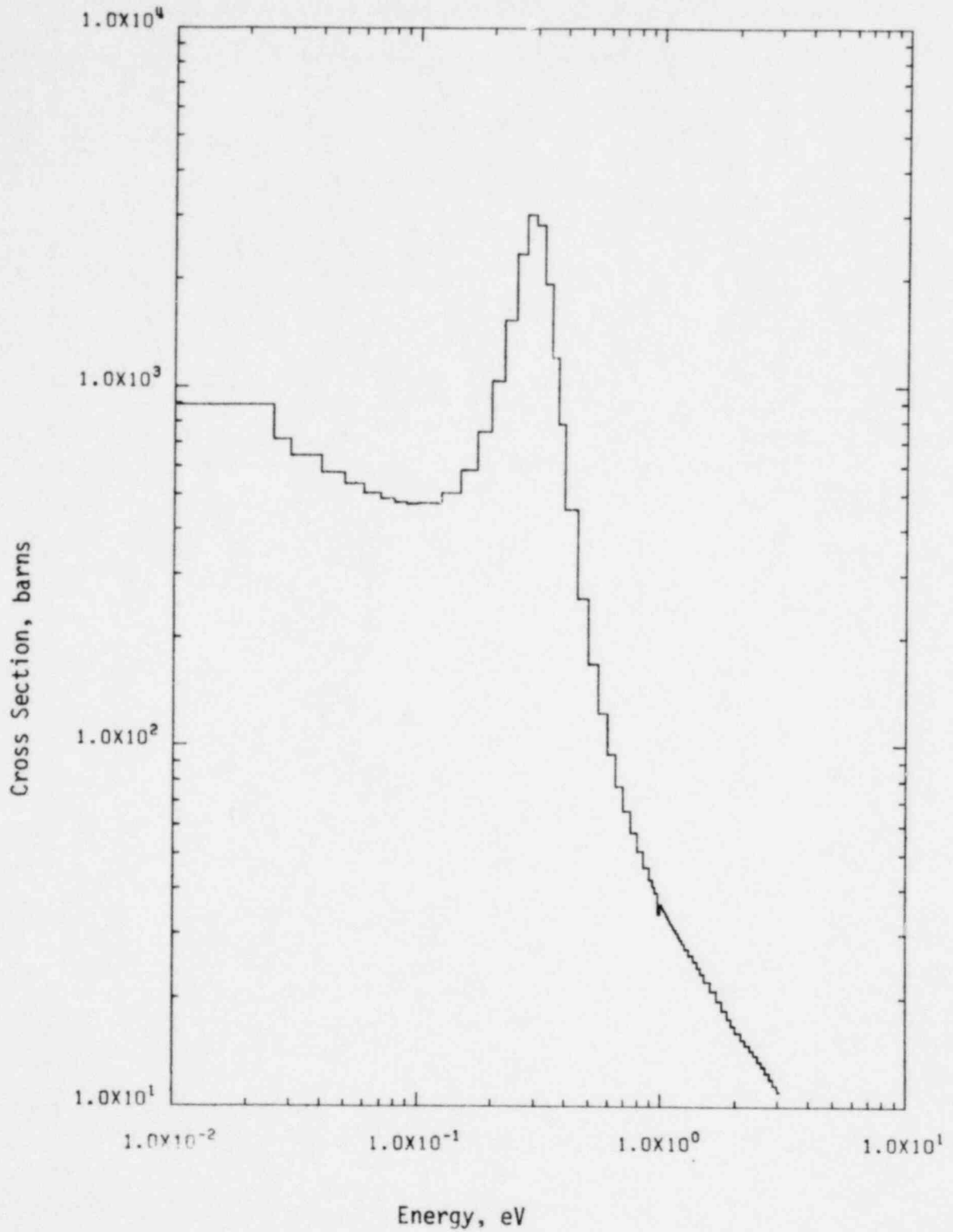


FIGURE 4. ENDF/B-IV Fission Cross Section for ^{239}Pu

POOR ORIGINAL

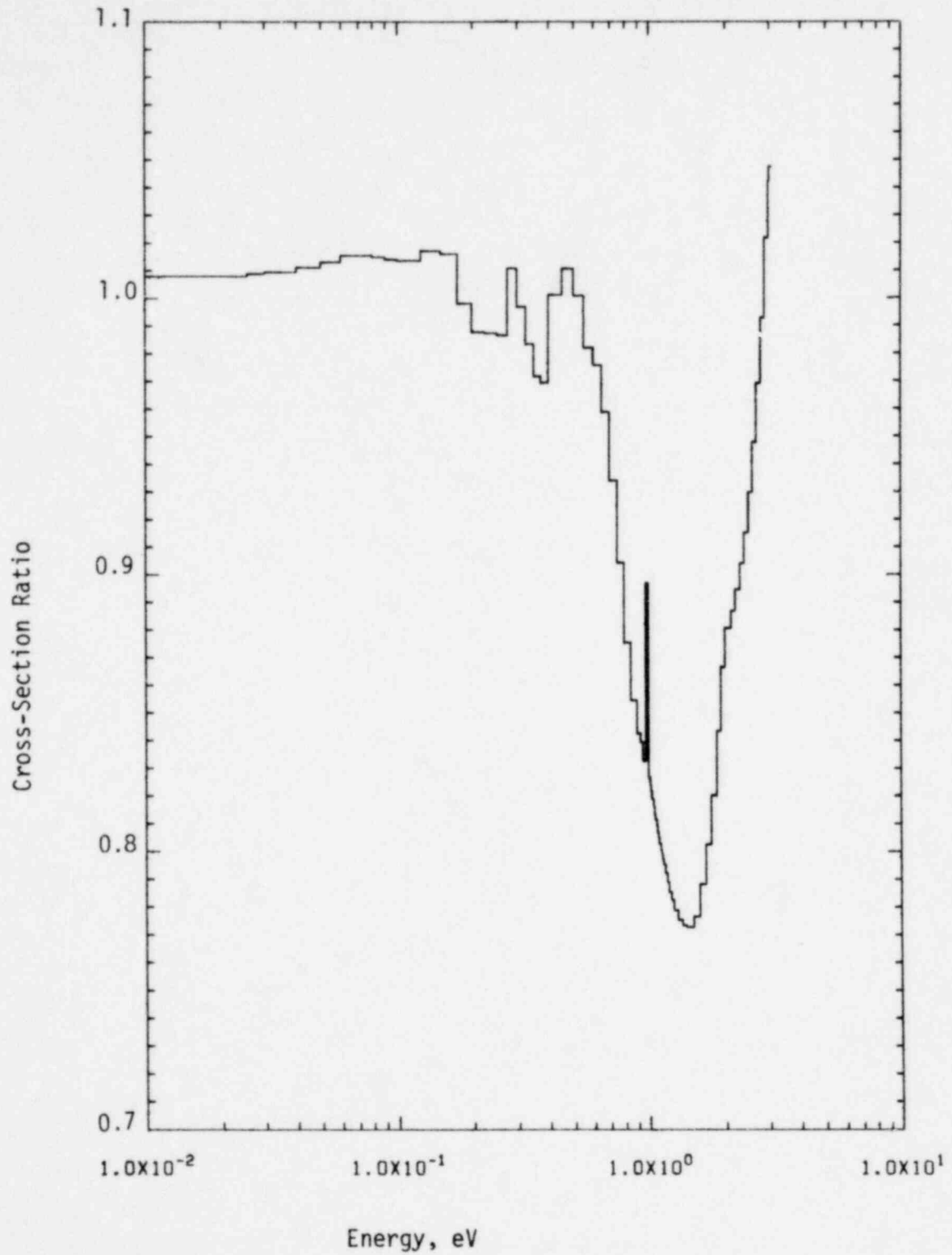


FIGURE 5. Ratio of New Data to ENDF/B-IV Data for ^{239}Pu Absorption

FOUR ORIGINAL

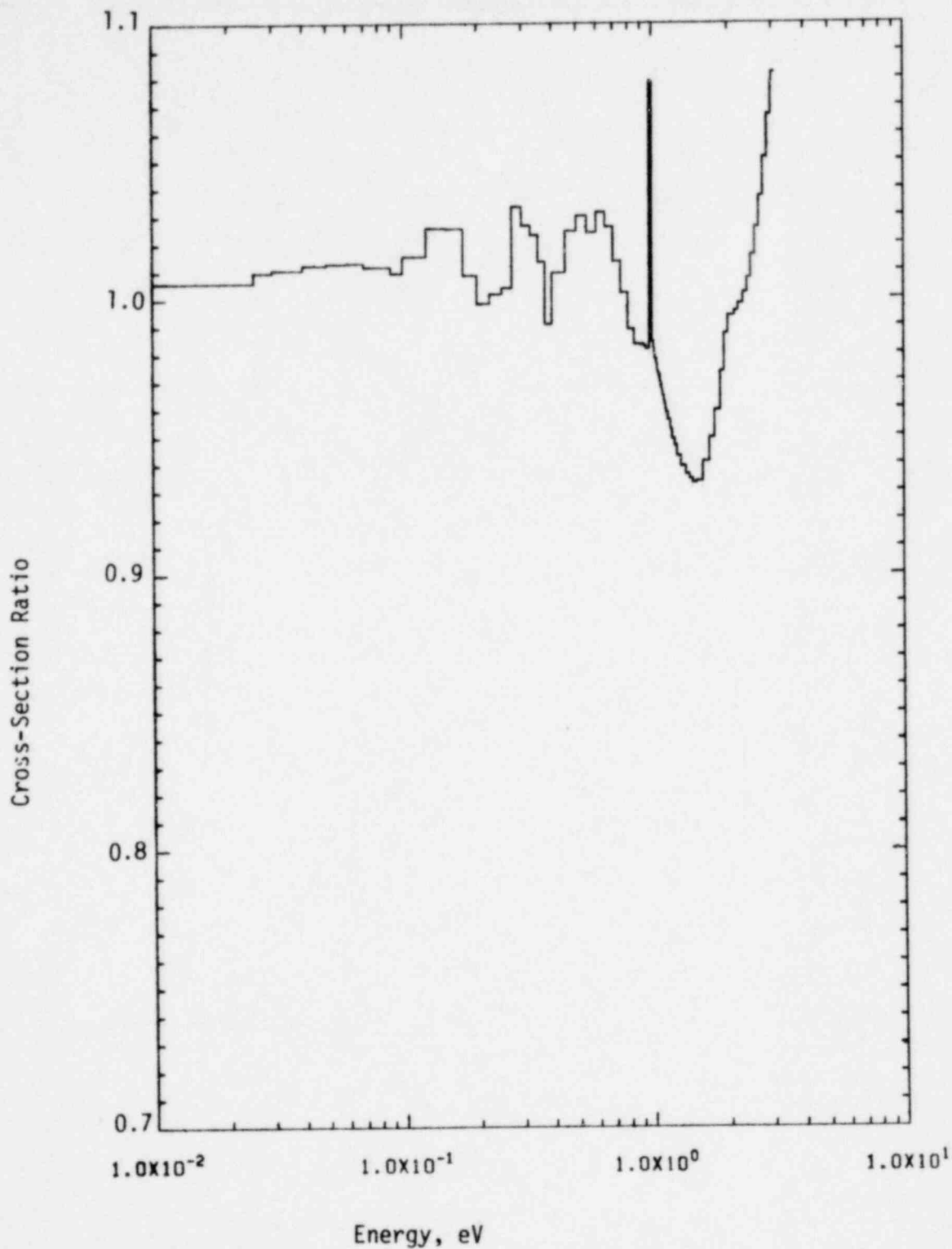


FIGURE 6. Ratio of New Data to ENDF/B-IV Data for ^{239}Pu Fission

996 154

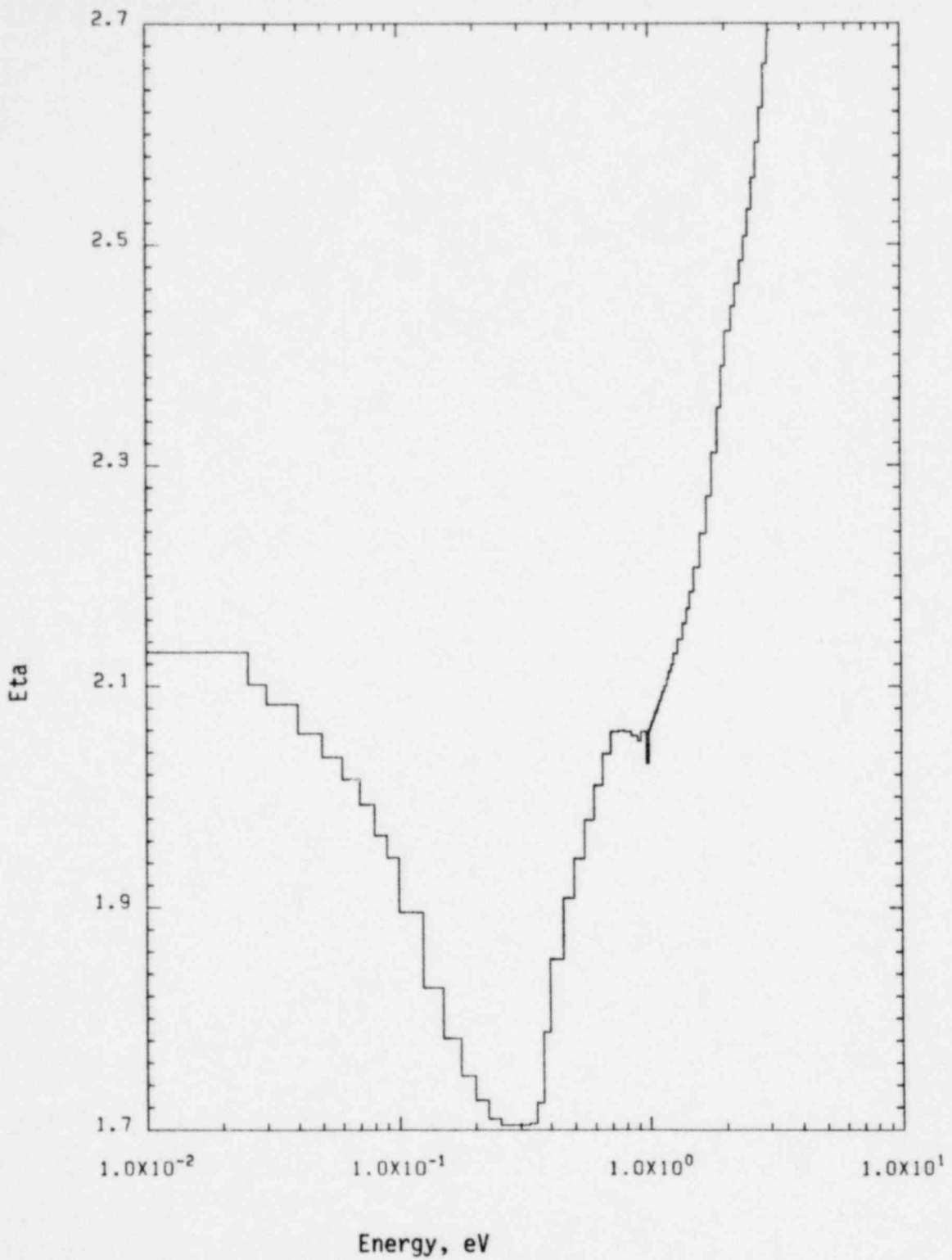


FIGURE 7. ENDF/B-IV Production-to-Absorption Ratio for ^{239}Pu

POOR ORIGINAL

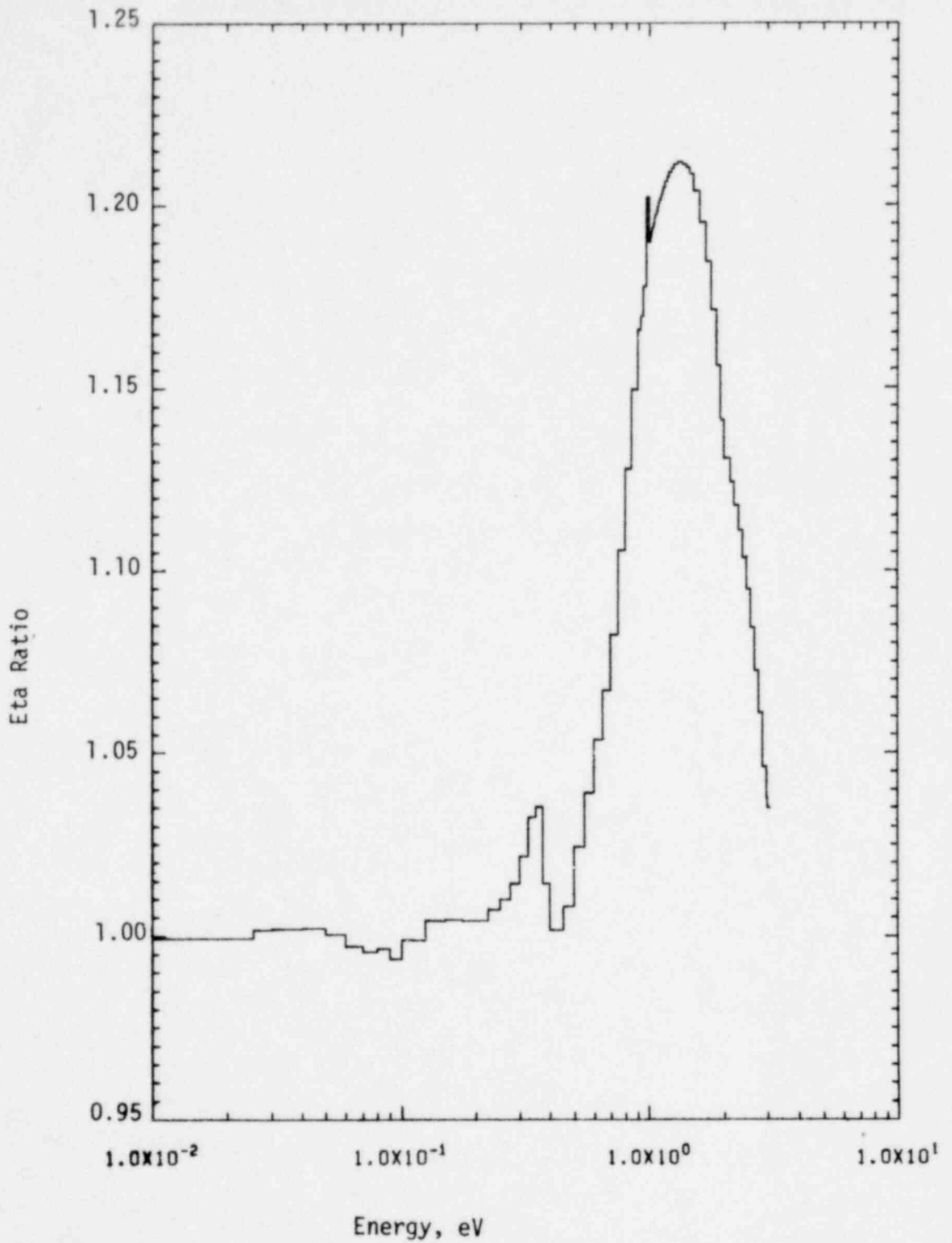


FIGURE 8. Ratio of Eta for New Data to Eta for ENDF/B-IV Data for ^{239}Pu

026-156

POOR ORIGINAL

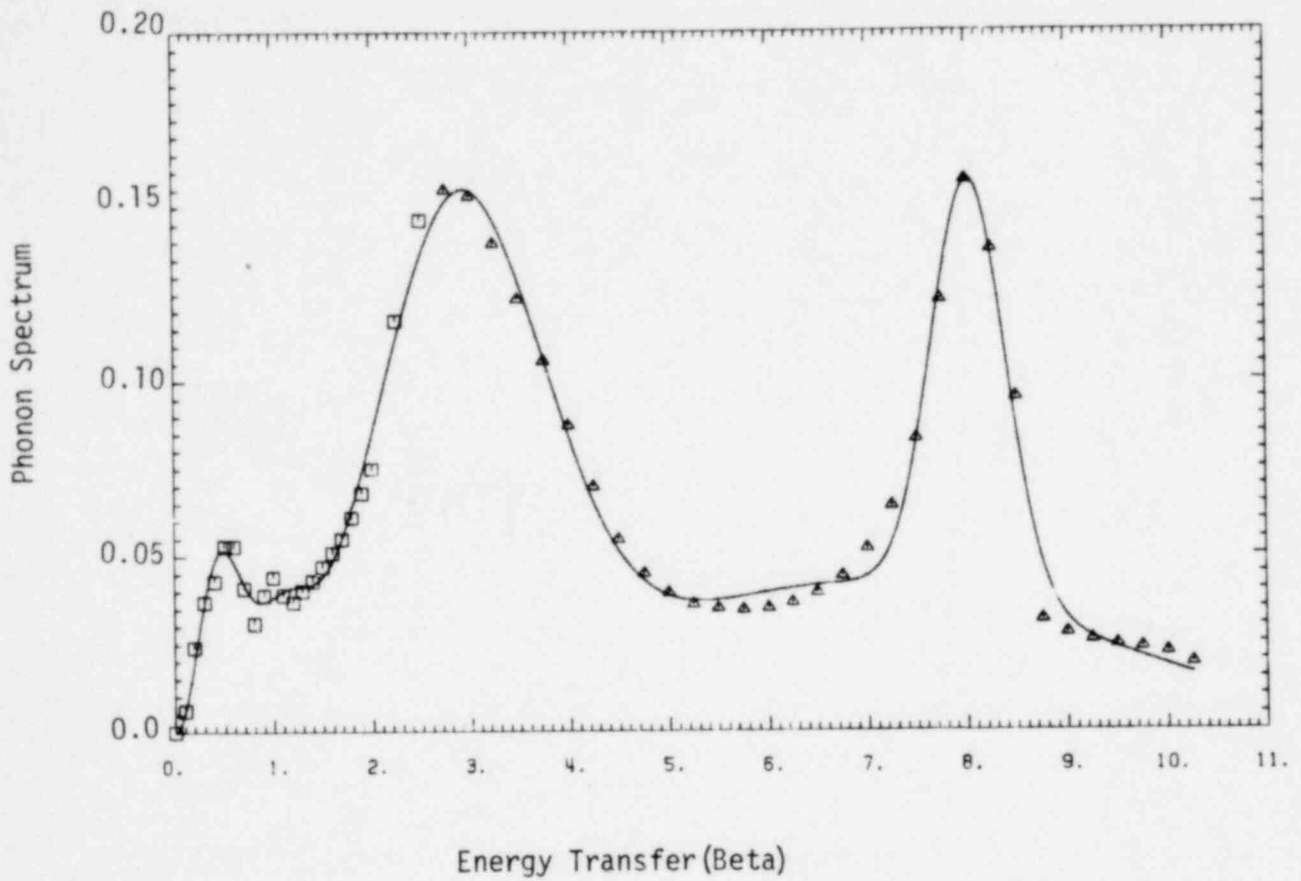


FIGURE 9. Phonon Spectrum Used to Evaluate the Scattering Law for Hydrogen Bond in Water

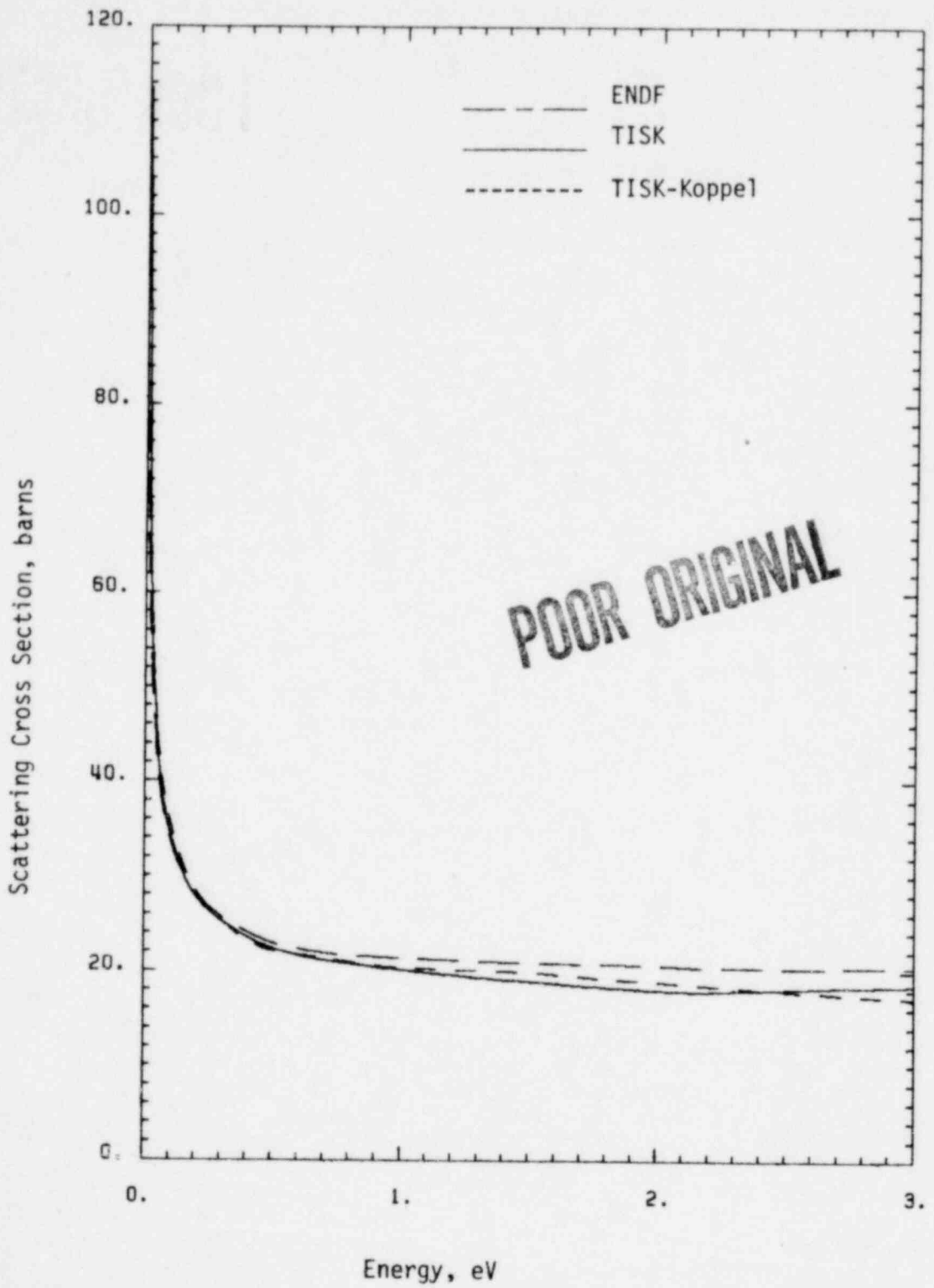


FIGURE 10a. Total Scattering Cross Section for Hydrogen Bound in Water

996 158

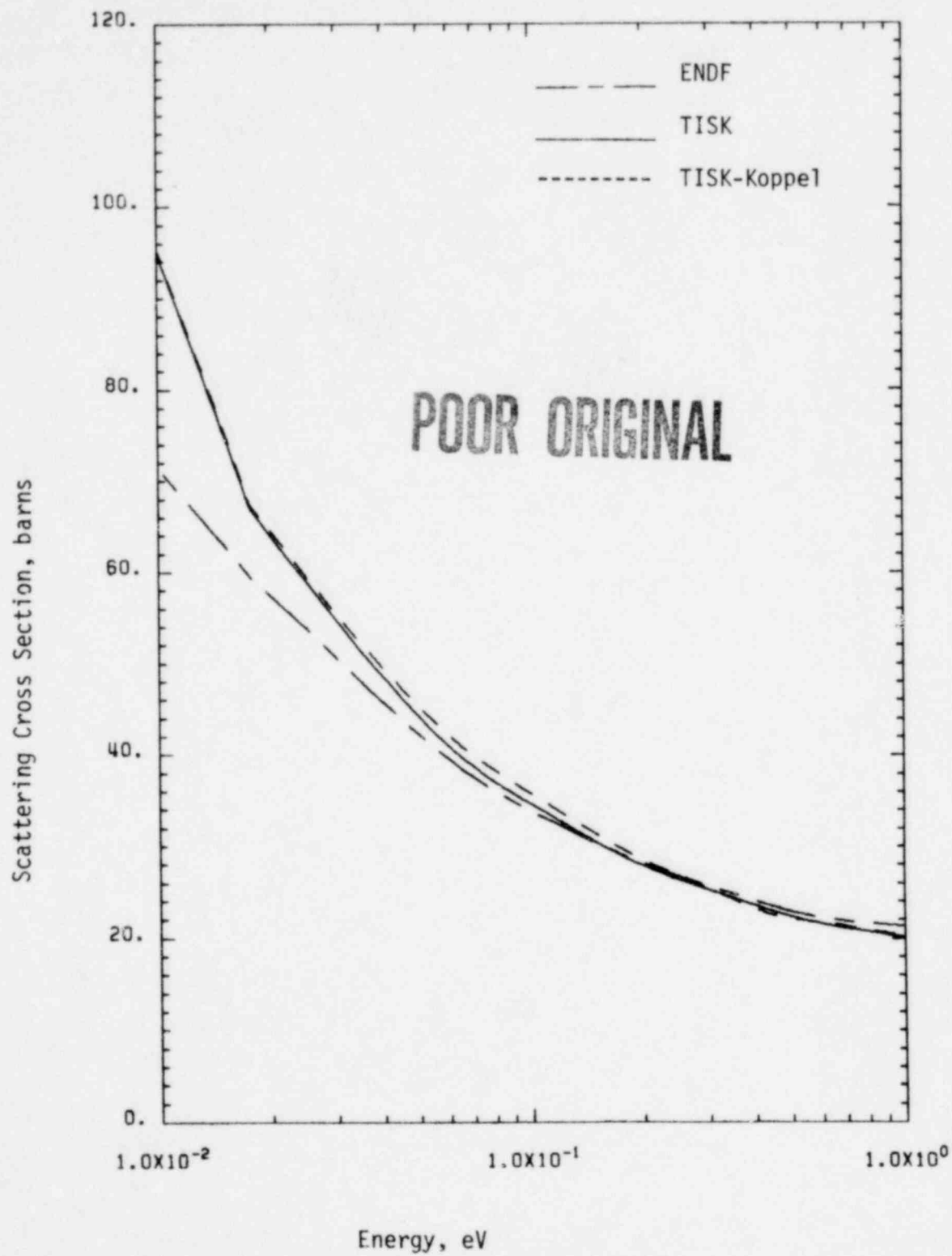


FIGURE 10b. Total Scattering Cross Section for Hydrogen Bound in Water

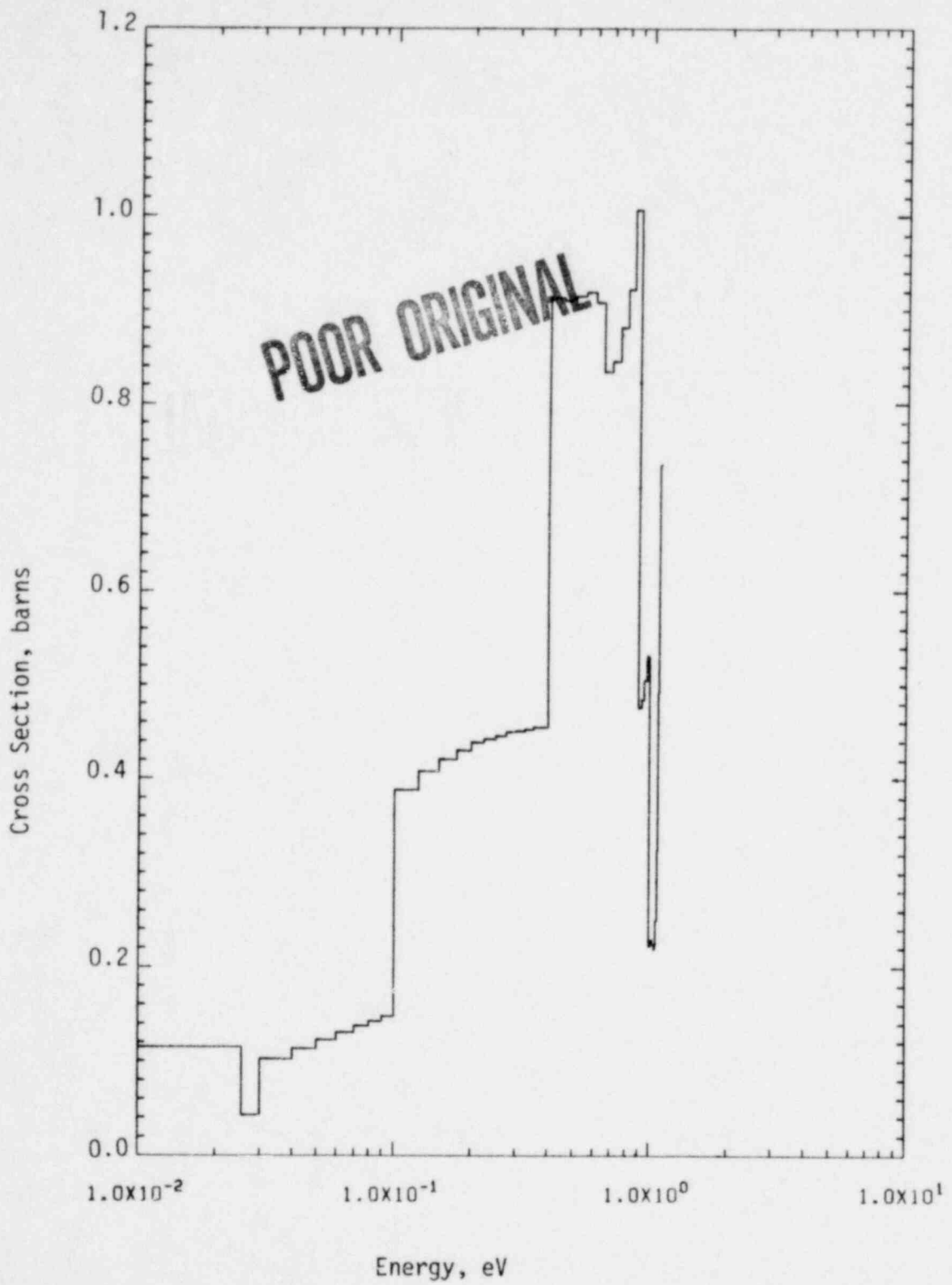


FIGURE 11. Transfer Cross Section from Group 173 for ENDF
Hydrogen Bound in Water

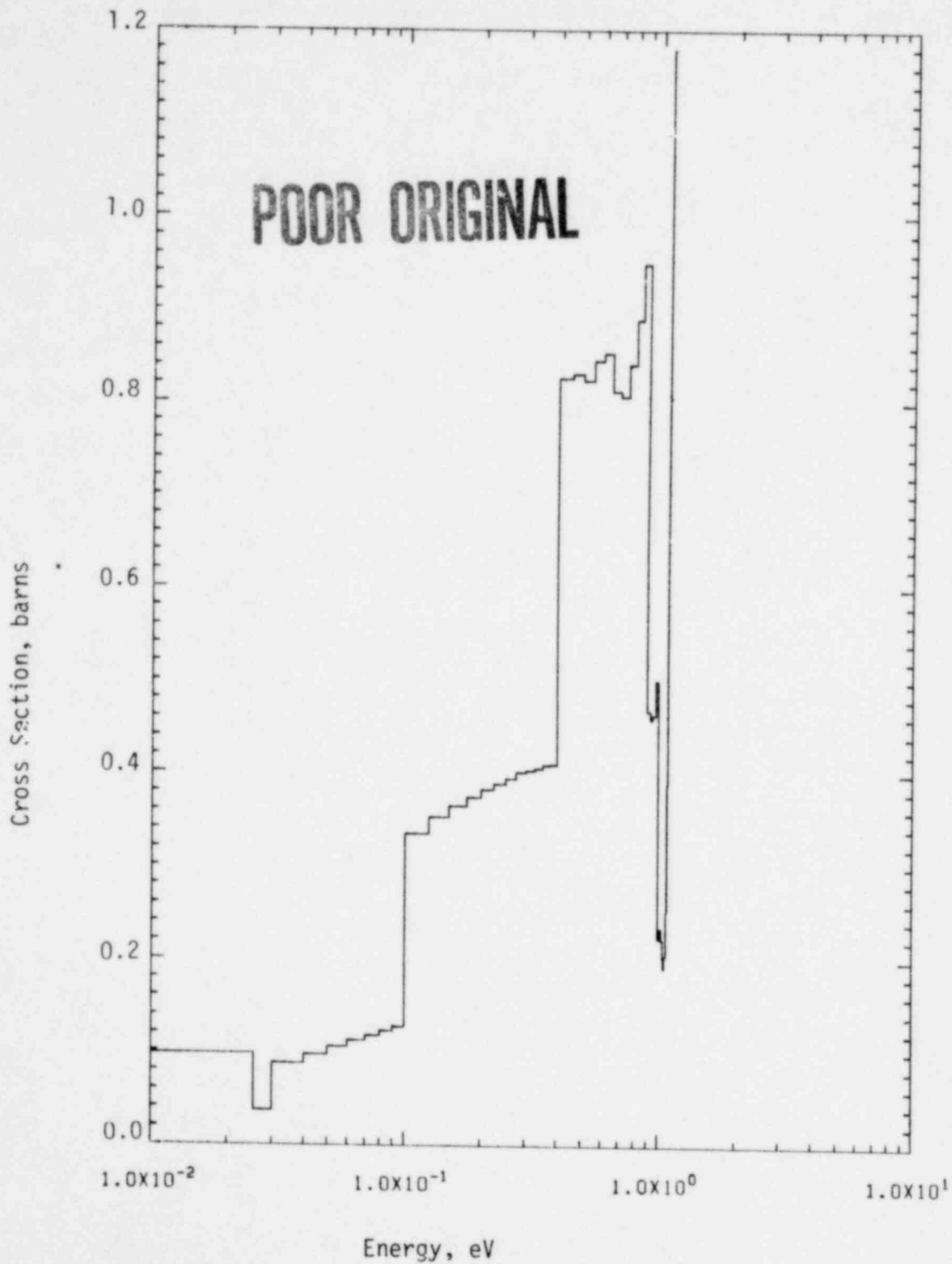


FIGURE 12. Transfer Cross Section from Group 173 for TISK
Hydrogen Bound in Water

996 161

POOR ORIGINAL

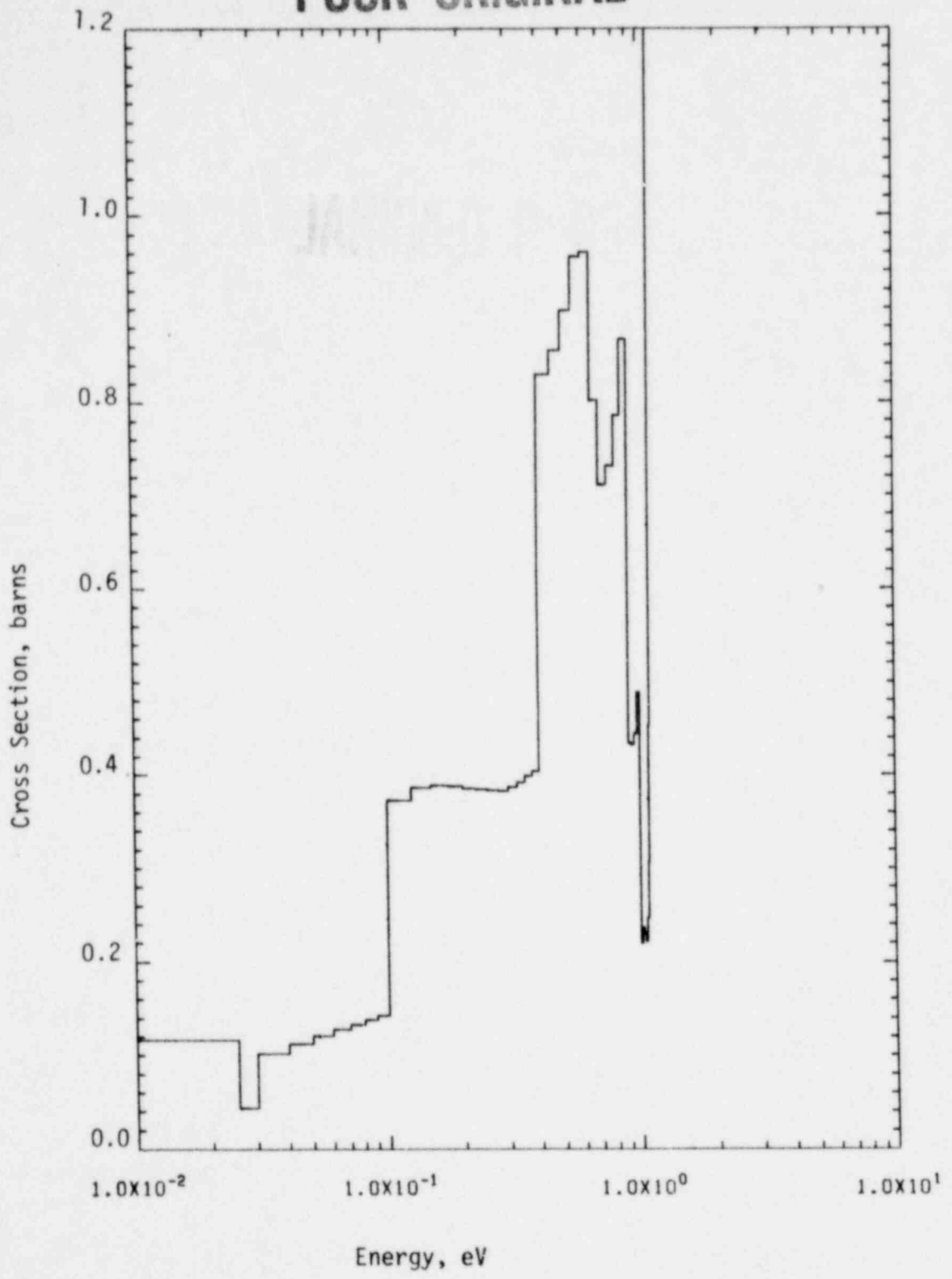


FIGURE 13. Transfer Cross Section from Group 173 for TISK-Koppel Hydrogen Bound in Water

996 162

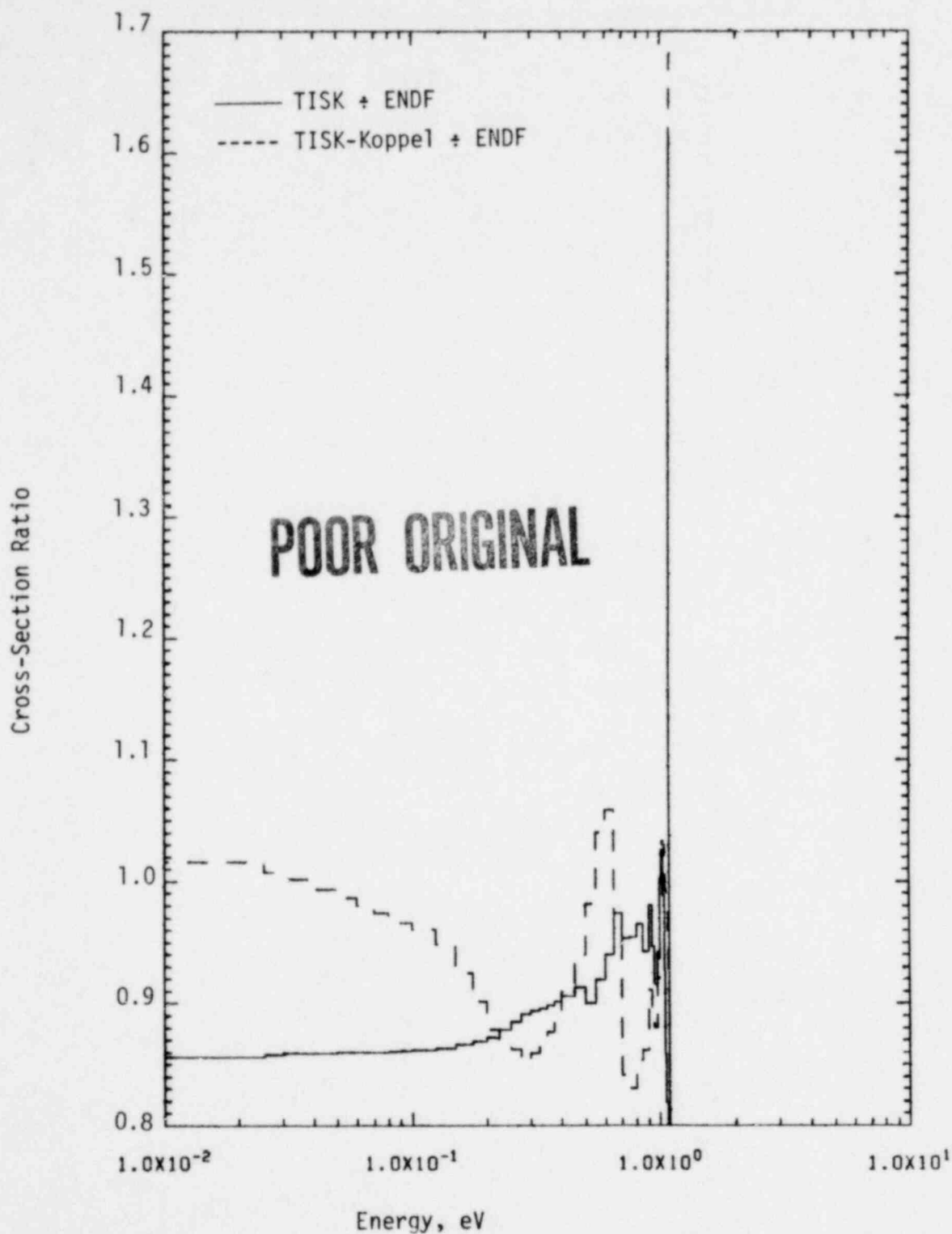


FIGURE 14. Ratio of Transfer Cross Sections from Group 173 for Hydrogen Bound in Water

996 163

POOR ORIGINAL

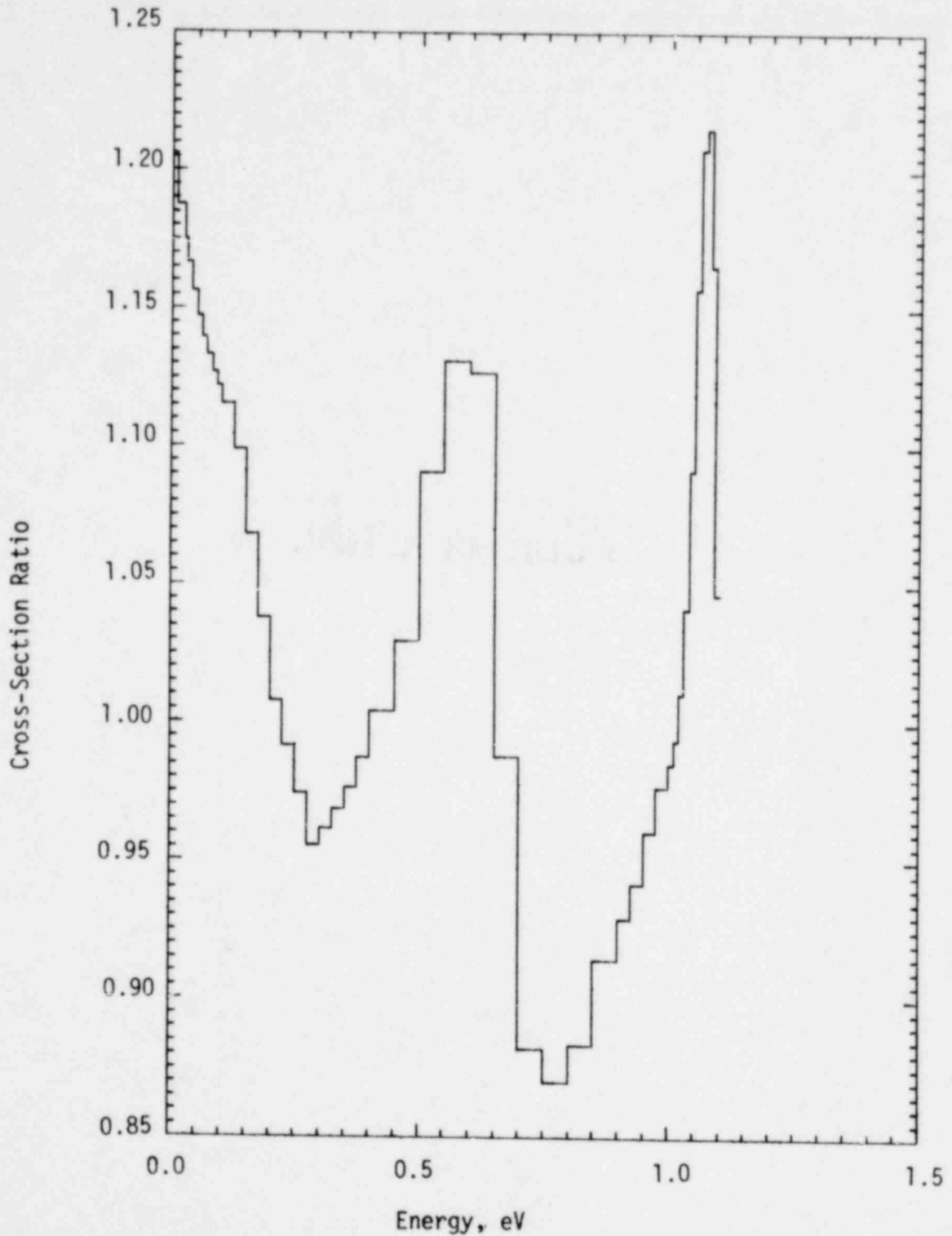


FIGURE 15. Ratio of TISK-Koppel to TISK Transfer Cross Sections from Group 173

POOR ORIGINAL

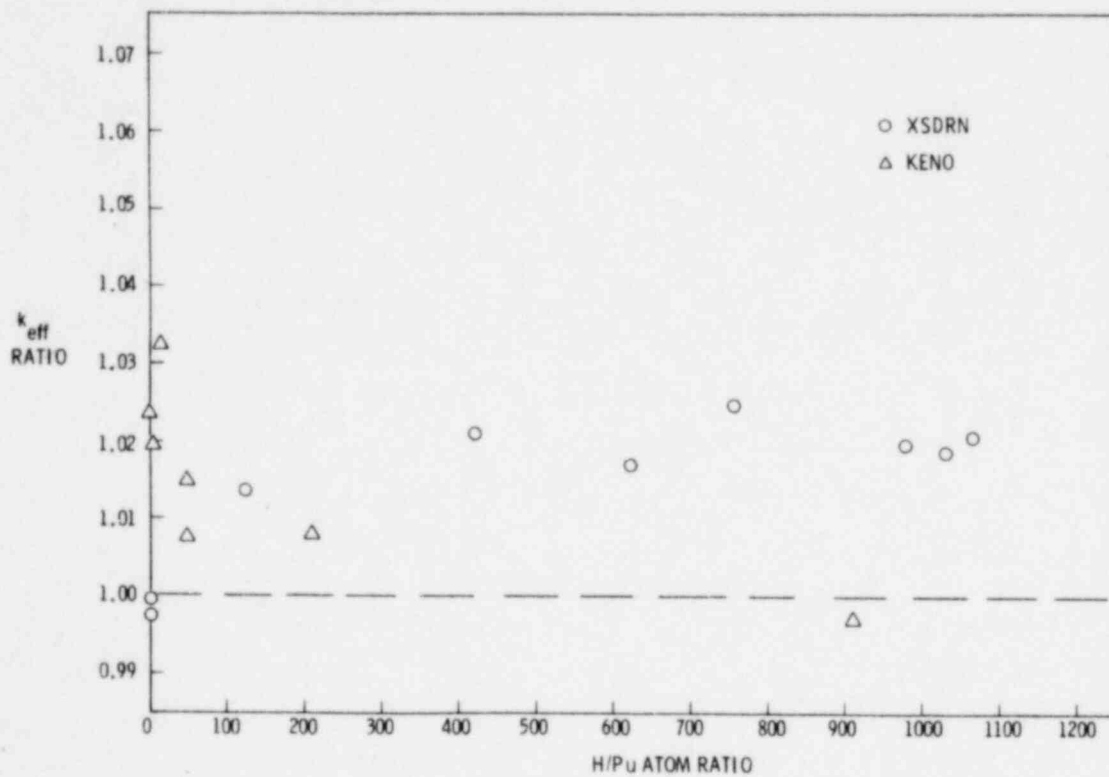


FIGURE 16. Reactivity of Homogeneous Plutonium Systems Using ENDF/B-IV Data

POOR ORIGINAL

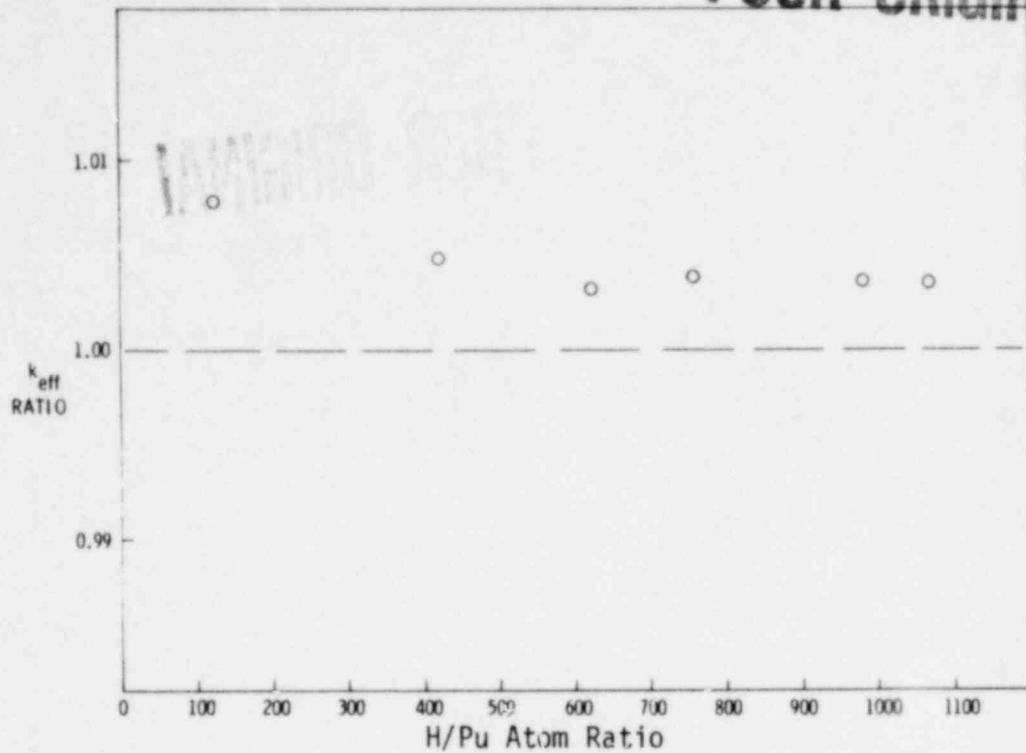


FIGURE 17. Reactivity Effect of New Data for ^{239}Pu

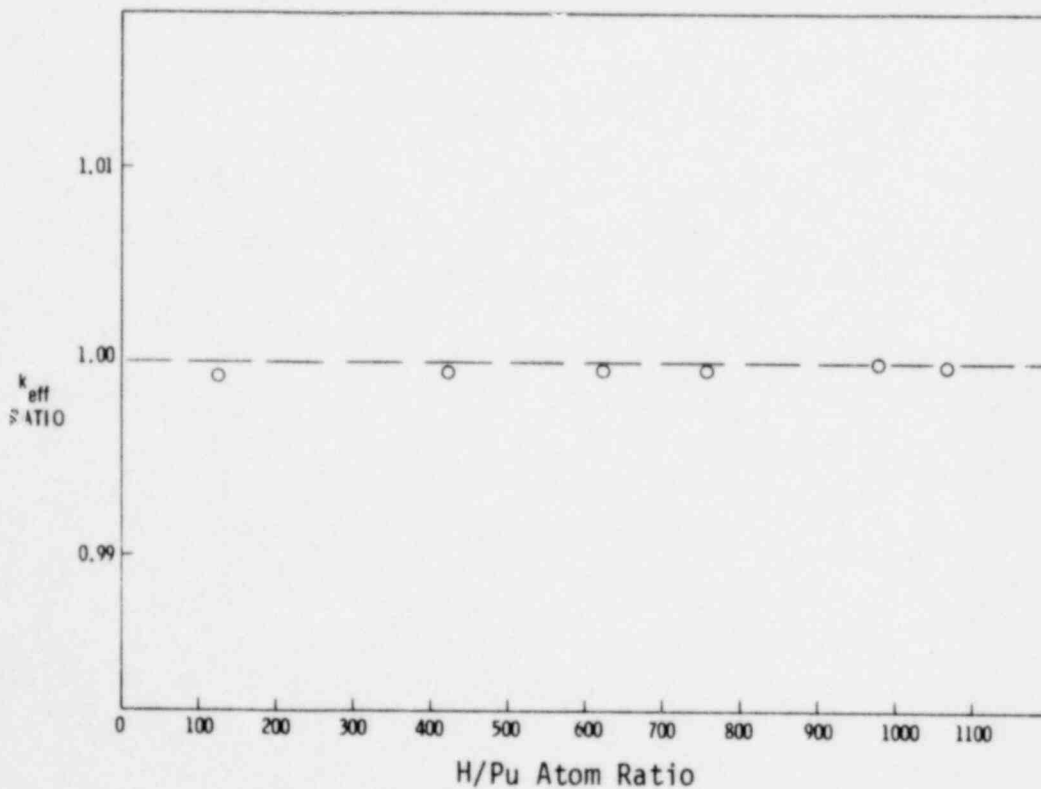


FIGURE 18. Reactivity Effect of New Data for ^{240}Pu

996 166

POOR ORIGINAL

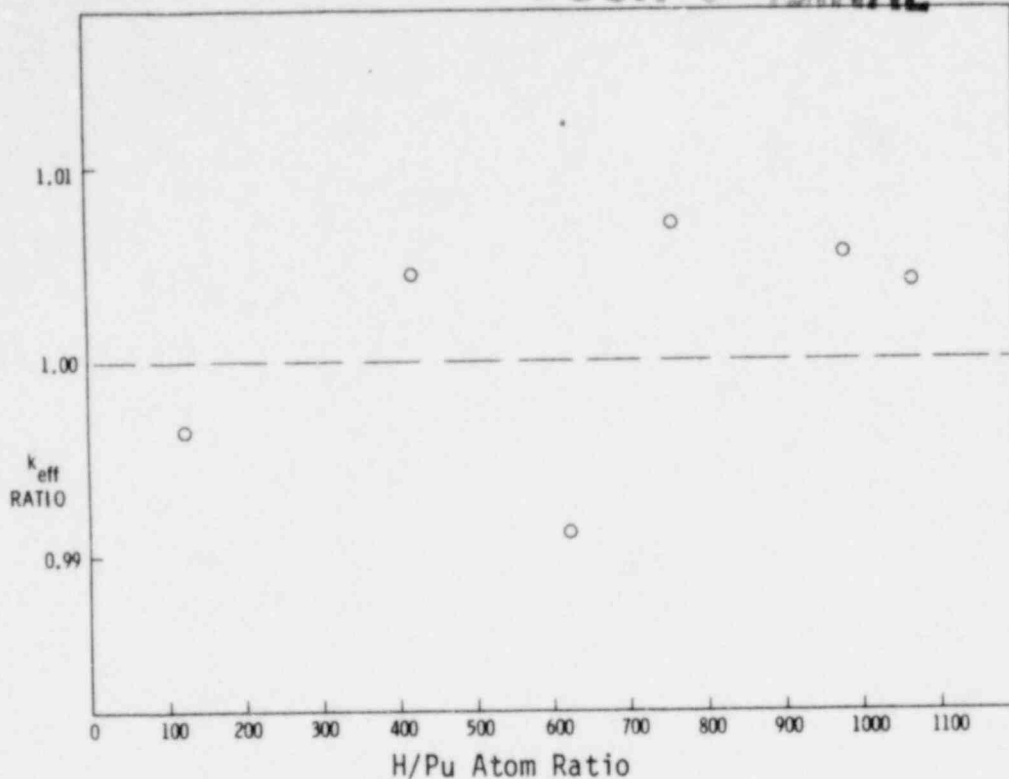


FIGURE 19. Reactivity Effect of Using TISK H₂O

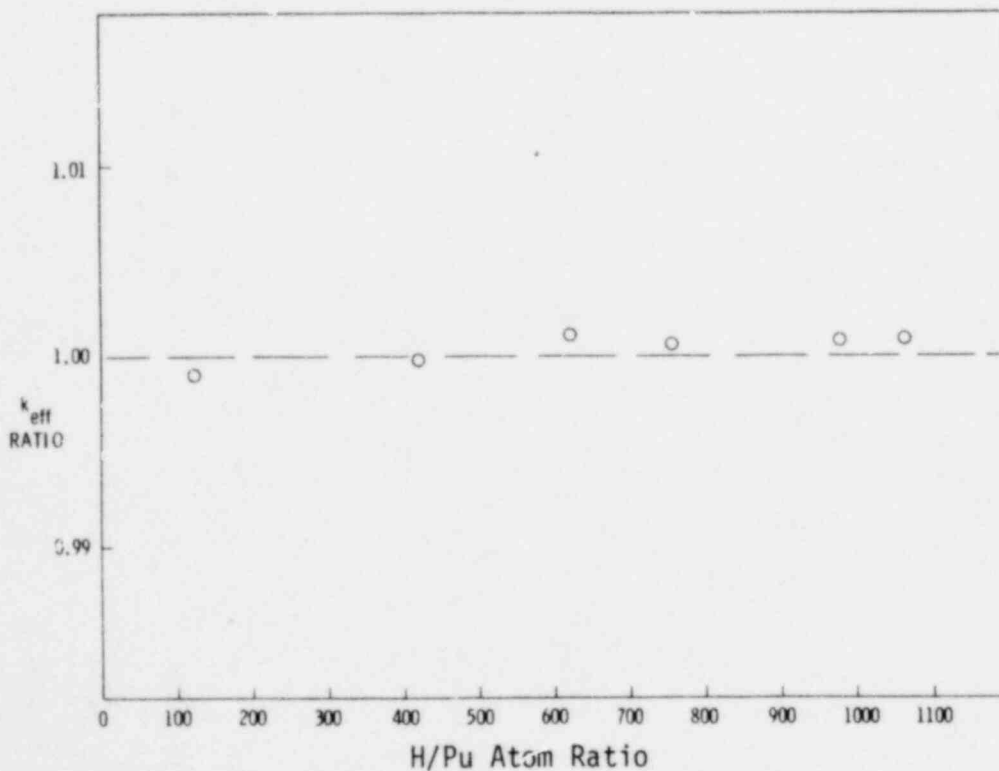


FIGURE 20. Comparison of TISK-Koppel to TISK

NRC FORM 335 (7-77)		U.S. NUCLEAR REGULATORY COMMISSION BIBLIOGRAPHIC DATA SHEET		1. REPORT NUMBER (Assigned by DDC) NUREG/CR-0965 PNL-3071	
4. TITLE AND SUBTITLE (Add Volume No., if appropriate) Integral Data Evaluation of Stainless Steel, ^{239}Pu , and H_2O for Homogeneous				2. (Leave blank)	
7. AUTHOR(S) UP Jerquin and others				3. RECIPIENT'S ACCESSION NO.	
9. PERFORMING ORGANIZATION NAME AND MAILING ADDRESS (Include Zip Code) Battelle Pacific Northwest Laboratory P.O. Box 999 Richland, WA 99352				5. DATE REPORT COMPLETED MONTH YEAR August 1979	
12. SPONSORING ORGANIZATION NAME AND MAILING ADDRESS (Include Zip Code) U.S. Nuclear Regulatory Commission Office of Nuclear Regulatory Research Division of Safeguards, Fuel Cycle and Environmental Research Washington, D.C. 20555				6. (Leave blank)	
13. TYPE OF REPORT Topical				7. (Leave blank)	
15. SUPPLEMENTARY NOTES				8. (Leave blank)	
16. ABSTRACT (200 words or less) <p>Theory-experiment correlations of plutonium-fueled systems using ENDF/B cross-section data have discrepancies which could be due to cross-section data, theoretical methods, and/or interpretation of the experiment. Analyses of homogeneous plutonium critical experiments were performed to determine where cross section deficiencies may exist. New thermal cross-section data (0.3 eV) were generated for ^{239}Pu and ^{240}Pu capture, fission, and neutrons per fission. Two scattering kernels for hydrogen bound in water were also generated. Calculated values of k_{eff} using this new data were compared with corresponding values using ENDF/B-IV data.</p> <p>The results indicate that the ^{240}Pu resonance data is sufficiently well known for hydrogen-moderated plutonium systems. In systems using stainless steel as structural and/or neutron control, a large fraction of the neutron absorptions occur in the stainless steel. Analyses of several systems containing stainless steel indicate that the uncertainty in calculated values of k_{eff} is small using current estimates of the uncertainties in the cross sections.</p>				10. PROJECT/TASK/WORK UNIT NO.	
17. KEY WORDS AND DOCUMENT ANALYSIS Nuclear Criticality Fuel shipment Fuel storage LWR				11. CONTRACT NO. B2075	
17b. IDENTIFIERS/OPEN-ENDED TERMS				13. PERIOD COVERED (Inclusive dates) N/A	
18. AVAILABILITY STATEMENT Unlimited				14. (Leave blank)	
19. SECURITY CLASS (This report) UNCLASSIFIED				16. SECURITY CLASS (This page) UNCLASSIFIED	
20. SECURITY CLASS (This page) UNCLASSIFIED				17. PRICE \$	
21. NO. OF PAGES 78				22. PRICE \$	

UNITED STATES
NUCLEAR REGULATORY COMMISSION
WASHINGTON, D. C. 20555

OFFICIAL BUSINESS
PENALTY FOR PRIVATE USE \$300

POSTAGE AND FEES PAID
U.S. NUCLEAR REGULATORY
COMMISSION



120555031837 2 ANRG
US NRC
~~SECY PUBLIC DOCUMENT ROOM~~
BRANCH CHIEF *Stewart Scott*
~~HSI LOBBY~~
WASHINGTON LA 212 DC 20555

POOR ORIGINAL

996 167